Title

Reprogramming sphingolipid glycosylation is required for endosymbiont persistence in Medicago truncatula

Journal

Current Biology, 31(11)

ISSN

0960-9822

Authors

Moore, William M
Chan, Candace
Ishikawa, Toshiki
et al.

Publication Date

2021-06-01

DOI

10.1016/j.cub.2021.03.067

Peer reviewed

Article

Current Biology

Reprogramming sphingolipid glycosylation is required for endosymbiont persistence in *Medicago truncatula*

Highlights

- Sphingolipid glycosyltransferases are differentially expressed in symbiotic tissues
- *MtGINT1* is expressed in cell types synthesizing perimicrobial membranes
- MtGINT1 functions in *N*-acetyl glucosamine sphingolipid glycosylation *in planta*
- Silencing *MtGINT1* impairs nodulation and arbuscular mycorrhizal symbiosis

Authors

William M. Moore, Candace Chan, Toshiki Ishikawa, ..., Maki Kawai-Yamada, Jenny C. Mortimer, Henrik V. Scheller

Correspondence

hscheller@lbl.gov

In brief

Plant endosymbioses with arbuscular mycorrhizal fungi and N_2-fixing bacteria rely on the formation of specialized cross-kingdom membrane interfaces. Here, Moore et al. show that changes in host sphingolipid glycosylation is important for development of perimicrobial membrane compartments and endosymbiont persistence within root cells.

Moore et al., 2021, Current Biology *31*, 2374–2385
June 7, 2021
https://doi.org/10.1016/j.cub.2021.03.067

CellPress

CellPress
OPEN ACCESS

Current Biology

Article

Reprogramming sphingolipid glycosylation is required for endosymbiont persistence in *Medicago truncatula*

William M. Moore,[1,2,3,9] Candace Chan,[1,2,5] Toshiki Ishikawa,[4] Emilie A. Rennie,[1,2,6] Heidi M.-L. Wipf,[1,2,3] Veronica Benites,[1,2,7] Maki Kawai-Yamada,[4] Jenny C. Mortimer,[1,2,8] and Henrik V. Scheller[1,2,3,10,*]

[1]Joint BioEnergy Institute, Emeryville, CA 94608, USA
[2]Environmental Genomics and Systems Biology Division, Lawrence Berkeley National Laboratory, Berkeley, CA 94720, USA
[3]Department of Plant and Microbial Biology, University of California, Berkeley, Berkeley, CA 94720, USA
[4]Graduate School of Science and Engineering, Saitama University, Saitama 388-8570, Japan
[5]Present address: University of California, San Francisco, San Francisco, CA 94143, USA
[6]Present address: Callisto Media, Emeryville, CA 94608, USA
[7]Present address: Checkerspot Inc, Berkeley, CA 94710, USA
[8]Present address: School of Agriculture, Food and Wine, University of Adelaide, Glen Osmond, SA, Australia
[9]Twitter: @moorrhizal
[10]Lead contact
*Correspondence: hscheller@lbl.gov
https://doi.org/10.1016/j.cub.2021.03.067

SUMMARY

Plant endosymbiosis relies on the development of specialized membranes that encapsulate the endosymbiont and facilitate nutrient exchange. However, the identity and function of lipids within these membrane interfaces is largely unknown. Here, we identify GLUCOSAMINE INOSITOL PHOSPHORYLCERAMIDE TRANSFERASE1 (GINT1) as a sphingolipid glycosyltransferase highly expressed in *Medicago truncatula* root nodules and roots colonized by arbuscular mycorrhizal (AM) fungi and further demonstrate that this enzyme functions in the synthesis of *N*-acetyl-glucosamine-decorated glycosyl inositol phosphoryl ceramides (GIPCs) *in planta*. *MtGINT1* expression was developmentally regulated in symbiotic tissues associated with the development of symbiosome and periarbuscular membranes. RNAi silencing of *MtGINT1* did not affect overall root growth but strongly impaired nodulation and AM symbiosis, resulting in the senescence of symbiosomes and arbuscules. Our results indicate that, although *M. truncatula* root sphingolipidome predominantly consists of hexose-decorated GIPCs, local reprogramming of GIPC glycosylation by MtGINT1 is required for the persistence of endosymbionts within the plant cell.

INTRODUCTION

Central to plant endosymbiosis is the synthesis of a specialized host-derived membrane that serves as an interface between the plant and the micro-organism. These membranes bear a symbiotic identity distinct from the plasma membrane based on protein composition[1,2] and are imperative for facilitating the bidirectional exchange of nutrients and information.[3–7] Moreover, they compartmentalize the micro-organism and are essential for the intracellular accommodation and persistence of the endosymbiont inside plant cells.[8,9] The synthesis of perimicrobial membranes is highly coordinated with the colonization and differentiation of the endosymbiont. Rhizobia and arbuscular mycorrhizal (AM) fungi enter plant cells through host-initiated asymmetric protrusions in the plasma membrane[10–12] that grow by means of targeted vesicle secretion and membrane fusion.[13,14] Although these symbioses culminate in vastly different morphological structures, they share a symbiosis-dedicated secretory pathway that drives the rapid growth of membrane around the endosymbiont,[15–17] the surface area of which increases 10- to 20-fold that of the plasma membrane and requires a massive amount of lipid synthesis. However, the molecular function of membrane lipids relative to the growth and maturation of the endosymbiotic compartment is unknown.

Early immunolabeling studies of nodules and AM-colonized roots identified glycolipid and glycoprotein epitopes enriched within perimicrobial membranes, which suggested that glycans may have important roles in symbiosis.[18–22] In particular, in pea (*Pisum sativum*), glycolipids were differentially distributed along the developmental gradient of the nodule.[22] One glycolipid, recognized by the monoclonal antibody JIM18, was specifically enriched in the membranes of young symbiosomes and infection threads but was strikingly absent from mature symbiosomes in the nitrogen fixation zone, coinciding with the boundary of starch accumulation.[22] JIM18 had antigenicity against a glucosamine, inositol, and phosphate-containing glycolipid that was resistant to mild alkaline hydrolysis, which is descriptive of a ceramide-containing glycosphingolipid.[23]

Glycosyl inositol phosphoryl ceramides (GIPCs) are highly glycosylated sphingolipids found in plants and fungi that are regarded as functional analogs of gangliosides in animal cells.[24] Plant GIPCs structure consists of ceramide lipid with a core glucuronic acid inositol phosphate headgroup (GlcA-IPC) that is further glycosylated with one or more sugars. The length and composition of the glycan head group is structurally diverse between plant species and is developmentally regulated in plant tissues.[25] GIPCs are major components of the plasma membrane, accounting for up to 25–40 mol% of total plasma membrane lipids,[26,27] and preferentially accumulate in the outer leaflet of the phospholipid bilayer, where they are believed to be involved in membrane organization, cell-surface interactions, and cell-signaling processes.[24,28] GIPCs are further enriched in detergent-insoluble membranes[26,29] and interact with phytosterols to form liquid ordered membrane domains or so called "lipid rafts."[30] However, the contribution of the glycan headgroup in these processes is not well understood.

Identification of GIPC glycosyltransferase mutants has demonstrated that GIPC glycosylation is critical for plant growth and development.[31–33] *Arabidopsis thaliana* GIPC MANNOSYL TRANSFERASE 1 (*gmt1*) mutants are highly dwarfed, with constitutively active defense response and cell adhesion phenotype,[32,34] and complete loss of GIPC glycosylation in *INOSITOL PHOSPHORYLCERAMIDE GLUCURONOSYL TRANSFERASE 1* (*iput1*) mutants is pollen lethal.[35,36] Similarly, *Oryza sativa* GLUCOSAMINE INOSITOL PHOSPHORYLCERAMIDE TRANSFERASE1 (*gint1*) mutants are severely dwarfed and seedling lethal.[31] GMT1 and GINT1 enzymes utilize the same GlcA-IPC substrate but produce distinct Man-GIPC and GlcN(Ac)-GIPC structures, respectively. Interestingly, monosaccharide substitution of *A. thaliana gmt1* mutants by cross complementation with *OsGINT1* only partially rescued the dwarfing phenotype, indicating that GIPC glycan sequences have intrinsic properties in plants. Recently, proteins secreted by necrotrophic plant pathogens have been shown to specifically target the glycan head group of GIPCs,[37] highlighting the importance of these moieties in conferring resistance or susceptibility to pathogenic micro-organisms.

Here, we identify *Medicago truncatula GINT1* as a glycosyltransferase-encoding transcript highly expressed in root nodules and roots colonized by arbuscular mycorrhizal fungi. We provide evidence to support that MtGINT1 functions in the synthesis of HexN(Ac)-GlcA-IPC structures *in planta*, consistent with the recently reported function of the *A. thaliana* and *O. sativa* GINT1 orthologs. Characterization of the *MtGINT1* promoter in hairy roots revealed that *MtGINT1* is expressed in nodule zones associated with symbiosome differentiation and in AM-colonized cortical root cells containing arbuscules. RNAi-mediated silencing of *MtGINT1* did not affect overall root growth but significantly impaired nodulation and AM symbiosis, resulting in the premature senescence of symbiosomes and arbuscules. Together, these results show that, although the *M. truncatula* root sphingolipidome primarily consists of hexose-decorated GIPCs, local production of HexN(Ac)-GIPC species within a symbiotic tissue-dependent context is necessary for the persistence of endosymbionts inside plant cells.

RESULTS

MtGINT1 expression is upregulated in symbiotic tissues

Medtr1g090920 was originally identified as a putative glycosyltransferase-encoding transcript (Mtr.43583.1.S1_at) highly upregulated in nodules and roots colonized by AM fungi (Figures S1A–S1C).[38–40] Phylogenetic analysis indicated Medtr1g090920 belonged to glycosyltransferase family 64 (GT64),[41] which was recently shown to function in GIPC glycosylation,[31,32] and clustered with GINT1 enzymes from *A. thaliana* and *O. sativa* (Figure 1A). GINT1 and GMT1 act as *N*-acetyl glucosaminyl- and mannosyl-transferases, respectively, and represent a major fork in the GIPC glycan biosynthesis pathway that produces distinct classes of GIPC (Figure 1B). We first measured the expression of *MtGINT1* and *MtGMT1* by qRT-PCR in *M. truncatula* roots in response to nutrient stress and symbiosis with either *Sinorhizobium meliloti* or *Rhizophagus irregularis* (Figures 1C and 1D). Results showed that *MtGINT1* expression was significantly upregulated in roots after inoculation with either *S. meliloti* or *R. irregularis* (Figure 1C). Interestingly, *MtGMT1* had the opposite expression profile and was significantly downregulated after either inoculation (Figure 1D).

The spatial expression pattern of *MtGINT1* was investigated by using ~2 Kb of upstream promoter to drive expression of different reporter constructs in transgenic hairy roots. In initial experiments, roots expressing *pMtGINT1:GUS* showed staining in the root tips of uninoculated plants and in nodules at 21 dpi (Figures S1D and S1E). GUS staining was also observed in young initiating nodules prior to root emergence (Figure S1F). Moving forward, fluorescent proteins were used as reporters to localize the expression of *MtGINT1* in live tissues. Roots expressing *pMtGINT1:YFP* showed intense YFP expression in nodules, with low or no fluorescence emanating from roots (Figure 1E). In hand-sectioned nodules expressing *pMtGINT1:mCherry-BCP1*,[42] a GPI-anchored plasma membrane marker, fluorescence was primarily detected in the infection zone and interzone, with minimal observable expression in the central nitrogen fixation zone (Figure 1F). This is in agreement with published laser capture microdissection (LCM) RNA sequencing (RNA-seq) data acquired from different nodule developmental zones (Figure S1B)[38] and consistent with immunostaining in pea nodules.[22] In root systems colonized by *R. irregularis*, the *pMtGINT1:BCP1-mCherry* reporter was expressed within zones of AM colonization, with little to no fluorescence emanating from the cortex of adjacent uncolonized root segments (Figures 1G and S1G).

We further investigated the cell-type specificity of *MtGINT1* expression by confocal laser scanning microscopy (CLSM) using a nuclear localized GFP construct. In AMF-colonized roots, *pMtGINT1:NLS-GFP* was co-expressed with *pMtBCP1:mCherry-BCP1*, under its native promoter, as a marker for arbuscule development.[42] The *MtGINT1* promoter was active in cells containing arbuscules, but not in adjacent uncolonized cells (Figure 1H). Albeit, the NLS-GFP reporter failed to exceed the nuclear pore size exclusion limit and localized to both the nucleus and dense cytoplasm surrounding the arbuscule trunk.[43] Activity of the *MtGINT1* promoter in these experiments was consistent with two published LCM transcriptomic studies, which have previously shown that *MtGINT1* is expressed in arbuscule-containing cells (Figure S1C).[39,40] In the context of nodulation, we

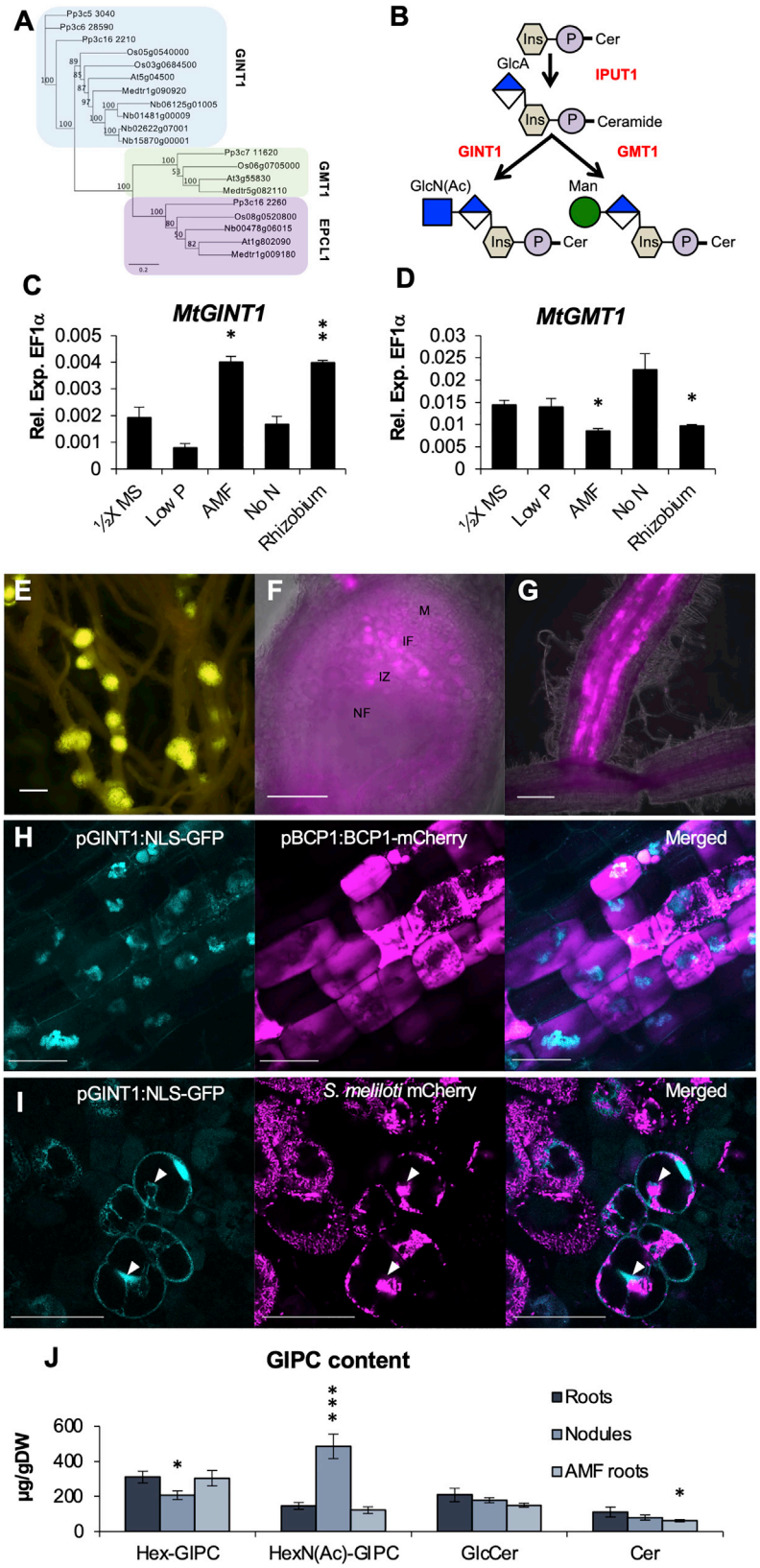

Figure 1. MtGINT1 is a GIPC GlcN(Ac)-glycosyltransferase expressed in symbiotic tissues

(A) Maximum likelihood tree of glycosyltransferase 64 family enzymes based on MUSCULE alignment with 100 bootstrap values.

(B) Known enzymes involved in GIPC glycosylation.

(C and D) Expression profiling of *MtGINT1* and *MtGMT1* by qRT-PCR in *M. truncatula* roots during nutrient stress and symbiosis. Plants were inoculated 21 days after germination and assayed at 28 dpi (mean ± SEM; n = 5).

(E) Expression of *pMtGINT1:YFP* in nodulated roots 21 dpi imaged under a fluorescence stereomicroscope.

(F) Hand-sectioned nodule expressing *pMtGINT1:SP-mCherry-BCP1* 21 dpi (scale bar represents 200 μm). Different nodule developmental zones are denoted: IF, infection zone; IZ, interzone; M, metistem; and NF, nitrogen fixation zone.

(G) Mycorrhized roots expressing *pMtGINT1:SP-mCherry-BCP1* 28 dpi with *R. irregularis* (scale bar represents 200 μm).

(H) Colocalization of *pMtGINT1:NLS-GFP* and arbuscule marker *pMtBCP1:SP-mCherry-BCP1* in roots 21 dpi with *R. irregularis*.

(I) Expression of *pMtGINT1:NLS-GFP* in the infection zone of nodules 21 dpi with *S. meliloti* expressing mCherry (arrows point to infection threads). Images in (H) and (I) reflect the maximal z-projection of 6 optical planes acquired by CLSM.

(J) GIPC content of uninoculated roots, dissected nodules 21 dpi, and mycorrhized root systems 28 dpi measured by LC-MS/MS (mean ± SEM; n = 5).

Asterisks indicate significant difference determined by Student's t test (*p < 0.05; **p < 0.01; ***p < 0.005). At, *Arabidopsis thaliana*; Mapoly, *Marchantia polymorpha*; Medtr, *Medicago truncatula*; Nb, *Nicotiana benthamiana*; Os, *Oryza sativa*; Pp, *Physcomitrella patens*. See also Figures S1 and S2.

carried out similar experiments using a *S. meliloti* strain expressing mCherry. Within the nodule infection zone, GFP fluorescence was present in cells containing infection threads and young symbiosomes (Figure 1I). Thus, *MtGINT1* is locally expressed in nodules and AM-colonized roots and in cell types synthesizing peribacteroid and periarbuscular membranes, respectively.

Sphingolipidomic survey of root tissues

Based on the differential expression levels of *MtGINT1* and *MtGMT1* in symbiotic tissues, we hypothesized that accompanying changes in sphingolipid composition would be associated with symbiosis. To test this, we carried out a liquid chromatography-tandem mass spectrometry (LC-MS/MS)-based analysis of glycosphingolipid content in uninoculated roots, excised nodules, and AM-colonized root systems (Figure 1J). Lipids from uninoculated roots contained both Hex-GIPC and HexN(Ac)-GIPC structures but predominantly consisted of the Hex variety, which constituted approximately 70% of the total GIPC pool (Figure 1J). Excised nodules had a 3.3-fold increase in HexN(Ac)-GIPC content and 1.5-fold decrease in Hex-GIPC content relative to uninoculated roots (Figure 1J), consistent with the pattern of *MtGINT1* and *MtGMT1* expression in these tissues (Figures 1C, 1E, and 1F). HexN(Ac) decorated GIPCs increased across all ceramide classes, with HexNAc t18:1-h16:0 being the most abundant sphingolipid in nodules (Figure S2A). Interestingly, we also found that the nodule GIPC pool predominantly contained hexosamine in the *N*-acetylated form (HexNAc), in contrast to uninoculated roots that primarily contained the deacetylated form (HexN; Figure S2A). Both Hex and HexN(Ac) GIPCs used the same ceramide bases in roots and nodules with preference for trihydroxylated 18:1 long-chain base with either a h16:0 or h24:0 fatty acid (Figures S2A–S2D). This illustrates that the only difference between these molecules is a single monosaccharide substitution in the glycan head group. Relative changes in GIPC composition could not be detected in AM-colonized root systems (Figures 1J and S2A). We speculate this was due to the heterogeneous nature of the material sampled and the low abundance of colonized cells relative to the total root system biomass. Furthermore, arbuscule development is non-synchronous and transient, which makes detecting relative changes in GIPC content challenging in these tissues.

MtGINT1 functions as a GIPC HexN(Ac)-transferase *in planta*

A. thaliana and *O. sativa* GINT1 orthologs have recently been characterized as GIPC *N*-acetyl glucosamine transferases.[31] To test whether this function is conserved in *M. truncatula*, we used LC-MS/MS to measure GIPC content in hairy roots expressing either *p35s:MtGINT1-RNAi* or *pAtUBQ3:MtGINT1*-overexpression constructs. *MtGINT1* silencing reduced total HexN(Ac)-GlcA-IPC content by 65% relative to control roots (Figure 2A) and impacted all HexN(Ac)-containing GIPC species; roots carrying *pAtUBQ3:MtGINT1* overexpression constructs had a 60% relative increase in total HexN(Ac)-GlcA-IPC content (Figure 2B). Overall changes in Hex-GlcA-IPC content were not significantly different in either experiment but had an opposite trend relative to *MtGINT1* expression (Figures 2C and 2D). To further confirm *MtGINT1* function as a GIPC HexN(Ac)-transferase, we ectopically overexpressed *MtGINT1* in *A. thaliana*, which completely lack HexN(Ac)-GIPC structures in vegetative tissues. Heterologous expression of MtGINT1 protein in *A. thaliana* resulted in non-native HexN(Ac)-decorated GIPCs in leaf tissue not detected in wild-type plants (Figures 2E and 2F). No growth phenotype was observed in the transformants. These results demonstrate that MtGINT1 functions in the glycosylation of HexN(Ac)-decorated GIPCs similar to the *O. sativa* and *A. thaliana* GINT1 orthologs.

MtGINT1 silencing impairs nodulation

We hypothesized that GIPC glycosylation by MtGINT1 functions in root nodulation symbiosis with *S. meliloti*. *MtGINT1* silencing by RNAi strongly impaired nodulation, resulting in small white nodules and chlorotic leaves consistent with a loss of symbiotic nitrogen fixation at 21 dpi (Figures 3A and 3B) but did not affect overall root growth under normal growth conditions (Figures S3A and S3B). Silencing efficiency of the *MtGINT1-RNAi* construct was measured by qRT-PCR and showed that target *MtGINT1* transcript abundance was reduced by 70% without significantly affecting *MtGMT1* expression (Figure 3C). Nitrogen fixation rates measured by acetylene reduction assay at 14 and 28 dpi confirmed that nitrogen fixation was significantly impaired in *MtGINT1-RNAi* nodules (Figure 3D). Furthermore, *MtGINT1* expression levels were positively correlated with the nitrogen fixation rate of nodules at 14 dpi (Figure 3E). Sphingolipid composition of excised nodules further showed that the *MtGINT1-RNAi* construct significantly decreased total HexN(Ac)-GIPC content (Figure 3F). Additionally, *MtGINT1*-silenced nodules did not accumulate the sphingolipid intermediates GlcA-IPC or ceramide but did show increased Hex-GIPC and glucosyl ceramide content, suggesting that sphingolipid intermediates enter other glycosylation pathways. Because nodules were able to form on *MtGINT1-RNAi* roots but remained small, white, and impaired in nitrogen fixation (nod+/fix−), we concluded that MtGINT1 is required for nodule development, but not for early perception or nodule initiation.

The nodulation phenotype associated with *MtGINT1* silencing was then investigated by light microscopy at 14 dpi. Semi-thin sections stained with Toluidine Blue O (TBO) revealed clear morphological defects in *MtGINT1-RNAi* nodules (Figures 3G–3J) compared to controls. Large amounts of membrane material were associated with releasing infection threads (Figure 3J, black arrows). Below, infected cells in the interzone contained many small vacuole-like structures and disorganized cellular contents, and symbiosomes in the nitrogen fixation zone appeared loosely packed and otherwise degraded (Figure 3J). Moreover, membranes and bacteroids in *MtGINT1-RNAi* nodules consistently stained violet relative to control nodules, which may indicate acidification of these tissues based on the metachromatic properties of TBO.[44] At least 50 sectioned nodules were examined per construct, yielding consistent phenotypic results.

A large amount of starch accumulation was also observed in the interzone of *MtGINT1-RNAi* nodules that was not present in corresponding controls (Figure 3J, white arrows). Fresh hand-sectioned nodules stained with potassium iodine showed starkly pronounced differences in starch distribution between control and *MtGINT1-RNAi* nodules (Figures 3K and 3L). At 21 dpi, control nodules accumulated starch in the nitrogen fixation

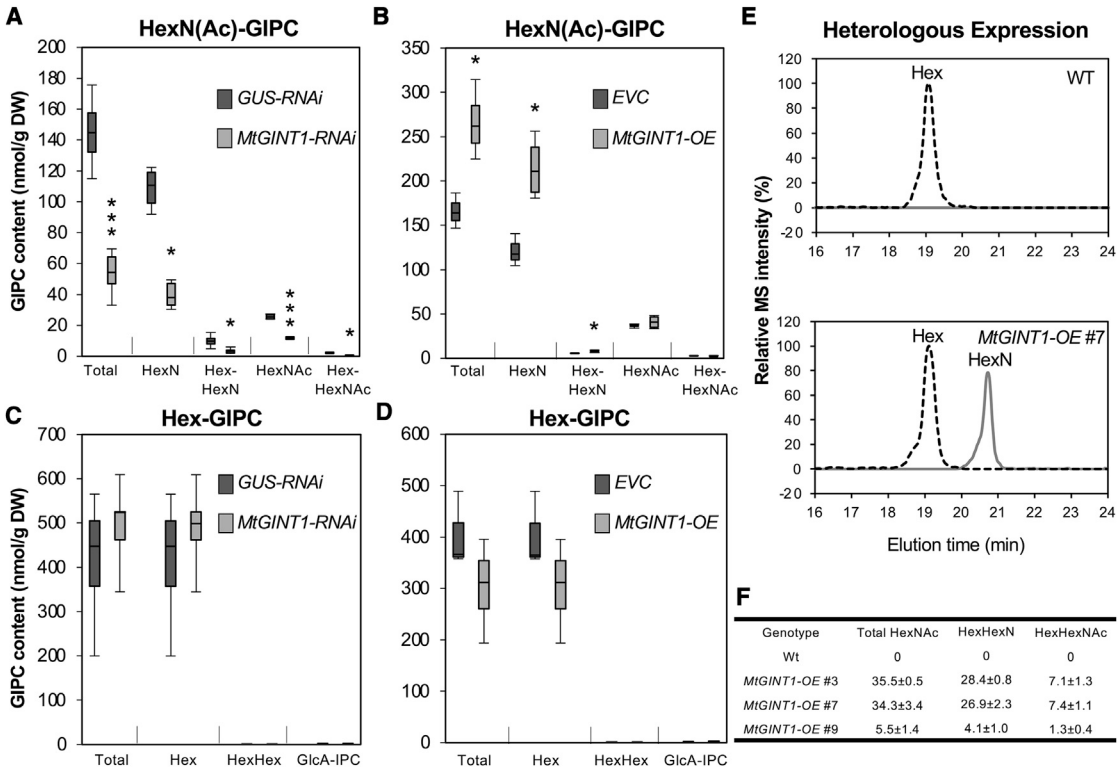

Figure 2. *MtGINT1* functions as a HexN(Ac) GIPC transferase *in planta*

(A and B) Boxplots representing HexN(Ac)-GIPC content measured by LC-MS/MS in *p35s:MtGINT1-RNAi* (A) and *pAtUBQ3:MtGINT1-OE* (B) roots compared to corresponding control roots.

(C and D) Hex-GIPC content in *p35s:MtGINT1-RNAi* (C) and *pAtUBQ3:MtGINT1-OE* (D) roots compared to controls was not affected (*MtGINT1-RNAi*, n = 6; *GUS-RNAi*, n = 4; *MtGINT1-OE*, n = 4; *EVC-OE*, n = 3).

(E) LC-MS/MS chromatograms targeting GIPCs with the Hex (blue dashed line, *m/z* 1260.8 > 662.6) or HexN (red solid line, *m/z* 1259.8 > 662.6) head group on t18:1-h24:1 ceramide backbone.

(F) HexN(Ac)-GIPC content of *A. thaliana* leaves from wild type and plants expressing *35 s:MtGINT1* constructs (mean ± SD; n = 6).

Data in (A)–(D) are presented in boxplots, and statistical significance was determined by Student's t test (*p < 0.05; **p < 0.01; ***p < 0.005).

zone in a pattern that clearly defined a developmental boundary with the interzone and the rest of the nodule apex (Figure 3K). This boundary was completely disrupted in *MtGINT1-RNAi* nodules, where starch accumulated in the infection zone and interzone and was absent from the nitrogen fixation zone (Figure 3L). These phenotypic observations were quantified in 50 hand-sectioned nodules stained with Lugol based on the presence or absence of the starch-defined boundary. Starch distribution was disrupted in all *MtGINT1*-silenced nodules examined, consistent with initial observations in plastic sections.

Nodulation phenotypes were further analyzed by live-cell confocal laser-scanning microscopy (CLSM) and transmission electron microscopy (TEM). CLSM experiments using mCherry-labeled *S. meliloti* produced similar results observed in TBO-stained, plastic embedded sections. Infection threads in *MtGINT1-RNAi* nodules were disorganized with an uncoordinated release of bacteria concomitant with altered symbiosome morphology and reduced bacterial fluorescence in the nitrogen fixation zone (Figures 3M and 3N). At the TEM level, large amounts of membrane debris aggregated at infection thread tips where *S. meliloti* released into disorganized clouds of nascent membrane, which appeared uncoordinated and non-adherent to the bacteria (Figures 3O and 3P). Prior to infection thread release, *S. meliloti* were noted to contain distinctly thick striated layers of extracellular material not seen in control nodules (Figure 3P). Below the infection zone, elongated bacteroids appeared highly degraded, with most cells being completely collapsed (Figures 3Q and 3R). Bacterial cell death was confirmed by live-dead staining using Syto 9 and propidium iodide, which confirmed that the majority of infected cells in *MtGINT1-RNAi* nodules contained senescent bacteria (Figures S3C and S3D). Each experiment originated from an independent round of root transformation, resulting in the same nodulation phenotype concomitant with the reduction of *MtGINT1* expression and HexN(Ac)-GIPC content. A Tnt-1 insertion line was ordered from the Noble Foundation (NF0903) but failed to yield any insertion in the *MtGINT1* locus in the seeds received. Based on the reproducible biochemical and phenotypic data, we concluded that RNAi-mediated silencing was sufficient for his study.

MtGINT1 silencing does not increase salicylic acid content or defense response

Mutations affecting GIPC glycosylation in *A. thaliana* trigger constitutive defense response characterized by increased

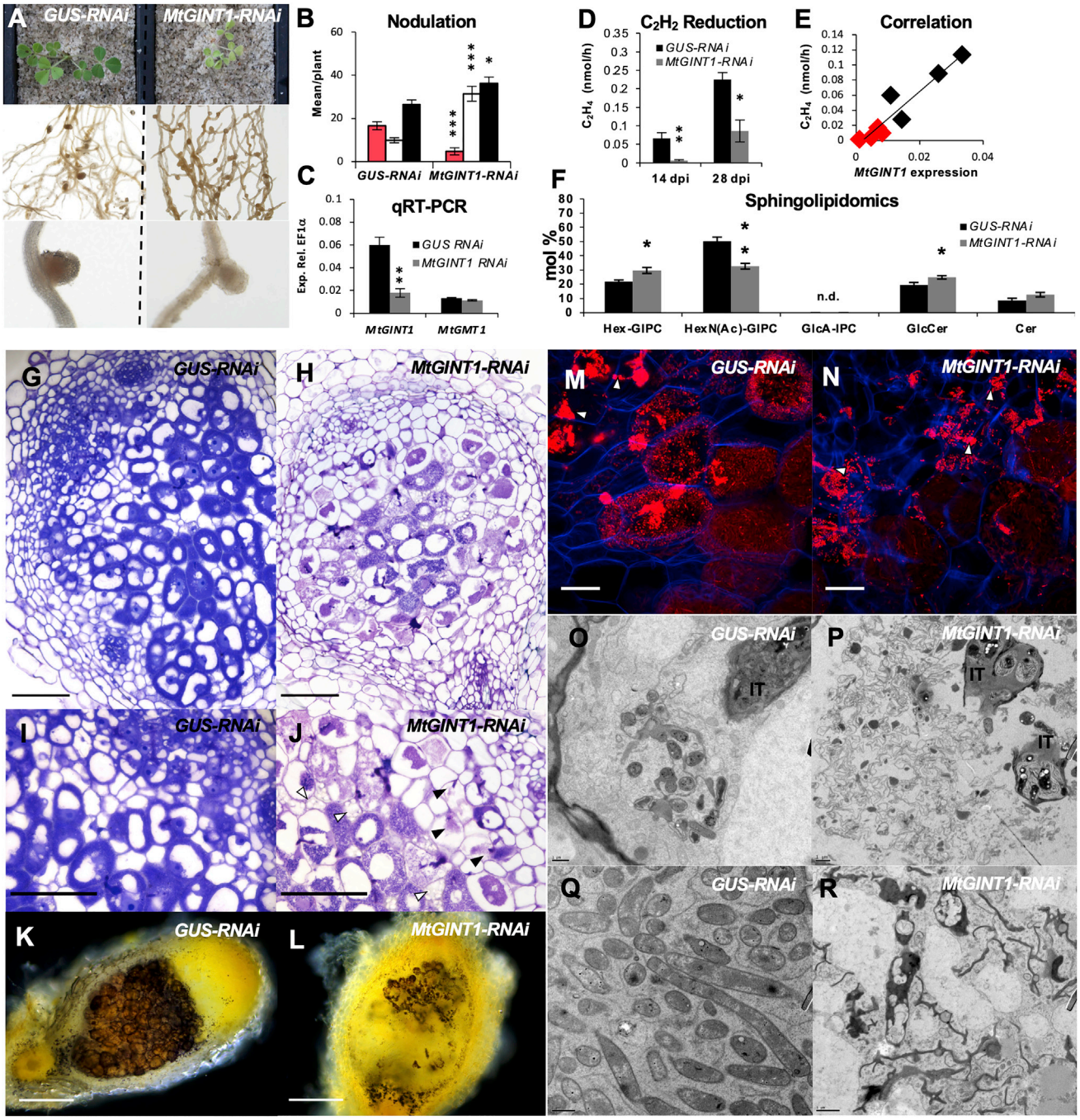

Figure 3. *MtGINT1-RNAi* silencing impairs nodulation and symbiosome development

(A) Shoots and transgenic root systems expressing *p35s:GUS-RNAi* (left) or *p35s:MtGINT1-RNAi* (right) constructs 21 dpi with *S. meliloti*.

(B) Mean number of nodules produced per root system categorized based on the visual presence or absence of leghemoglobin (white, immature; pink, mature; black, total) at 21 dpi ± SEM (n = 12).

(C) Expression of *MtGINT1* and *MtGMT1* in RNAi nodules 21 dpi measured by qRT-PCR relative to *MtEF-1α*; mean ± SEM (n = 4).

(D) Nitrogen fixation efficiency measured by acetylene reduction assay; mean ± SEM (n = 5, 14 dpi; n = 3, 28 dpi).

(E) Correlation between *MtGINT1* expression and nitrogen fixation efficiency in RNAi nodules 14 dpi (red, *MtGINT1-RNAi*; black, *GUS-RNAi*).

(F) Sphingolipid composition of excised RNAi nodules 21 dpi measured by LC-MS/MS; mean ± SEM (n = 4).

(G–J) Light microscopy images of plastic embedded nodule sections (4 μm thick) stained with Toluidine Blue O 14 dpi (scale bar represents 100 μm). Black arrows point to membrane material around infection threads, and white arrows point to starch in *MtGINT1-RNAi* nodules.

(K and L) Lugol starch staining in *GUS-RNAi* and *MtGINT1-RNAi* nodules 21 dpi (scale bar represents 250 μm).

(M and N) Live-cell CLSM images of hand-sectioned *GUS-RNAi* (M) and *MtGINT1-RNAi* (N) nodules 21 dpi with mCherry fluorescent *S. meliloti* (scale bar represents 50 μm). White arrows point to releasing infection threads.

(legend continued on next page)

H_2O_2 and salicylic acid (SA) and ectopic cell death.[31,32,36,45] Sphingolipid metabolism and SA signaling are intrinsically linked through the accumulation of bioactive lipid intermediates, such as ceramide and phytosphingosine, which play a role in triggering SA-dependent hyper-sensitive response to plant pathogens.[46–50] Therefore, we hypothesized that the bacterial cell death phenotype in *MtGINT1-RNAi* nodules could be caused by heightened defense response. Nodules 21 dpi stained with 3,3′-diaminobenzidine (DAB) showed increased H_2O_2 in *MtGINT1-RNAi* nodules relative to control nodules (Figures S3E and S3F). SA content was then measured by LC-MS/MS in *RNAi* roots that were either mock inoculated or 21 dpi with *S. meliloti* (Figure S3G). *MtGINT1* silencing had no effect on SA content in mock inoculated roots. Surprisingly, however, nodulated *MtGINT1-RNAi* roots had less SA content than corresponding nodulated control roots. Lastly, the expression of defense and senescence-associated genes were measured by qRT-PCR in nodules to further ascertain whether defense responses were elicited by *MtGINT1* silencing (Figure S3H). NDR1 (Medtr5g076170), which acts downstream of SA, was significantly reduced in nodulated *MtGINT1-RNAi* roots consistent with the biochemical SA measurements. The expression of a defense-related chitinase gene (Medtr3g118390), previously shown to be upregulated in nodules with constitutively active defense response,[51] was also significantly reduced in *MtGINT1-RNAi* roots. We also measured the expression of two cysteine proteases (Medtr5g022560 and Medtr4g079800) associated with normal programmed nodule senescence[52] but did not detect significant differences. Expression of two antimicrobial peptides, NCR169 and NCR211, important for bacteroid differentiation,[52,53] were also reduced in *MtGINT1-RNAi* nodules. Based on these results, we concluded that the bacterial cell death and H_2O_2 accumulation phenotype of *MtGNIT-RNAi* nodules is not caused by increased SA or defense-related gene expression.

MtGINT1 silencing impairs AM symbiosis

We hypothesized that MtGINT1 may also function in AM symbiosis based on its expression pattern in arbuscule-containing cells and the strong nodulation phenotype imparted by *MtGINT1* silencing. Hairy roots expressing either *pAtUBQ3:MtGINT1-RNAi* or empty vector control constructs were inoculated with *R. irregularis* and assayed at 12 and 28 dpi. At both time points, the infection frequency (F%), total mycorrhization (M%), and arbuscule abundance (A%) were significantly reduced in *pAtUBQ3:MtGINT1-RNAi* roots relative to empty vector control roots (Figure 4A). Arbuscule density within colonized root fragments was also reduced, and fewer mature arbuscules (ma%) were observed (Figure 4B). The majority of arbuscules formed in *MtGINT1-RNAi* roots appeared stunted (da%), and a stark increase in hyphal septation (s%) was observed (Figures 4B–4F). Similar results were obtained in a separate experiment using *35 s:MtGINT1-RNAi* constructs assayed at 35 dpi (Figure S4). Expression of the arbuscule-specific phosphate transporter *MtPT4* and the *R. irregularis* elongation factor *RiTEF* were measured by qRT-PCR as independent markers for arbuscule abundance and fungal biomass, respectively.[54] Expression of both genes was significantly reduced in *MtGINT1-RNAi* roots, consistent with microscopic observations (Figures 4G and 4H). *MtGINT1* expression was efficiently silenced by the *pAtUBQ3:MtGINT1-RNAi* construct (Figure 4K), without significantly affecting *MtGMT1* expression (Figure 4K). Lastly, expression of *MtMYB1*, the master transcriptional regulator of arbuscule degradation,[55] was measured to test whether *MtGINT1* silencing activated programmed arbuscule senescence. Expression of *MtMYB1* was significantly reduced in *MtGINT1-RNAi* roots at both time points relative to control roots (Figure 4I). These results indicate that the senescent AM phenotype in *MtGINT1-RNAi* roots was not a result of programmed arbuscule senescence and could be more attritubted to alterations in membrane biophysical properties.

DISCUSSION

Plant endosymbiosis relies on the development of a host-derived membrane compartment that is essential for the growth, differentiation, and persistence of the endosymbiont inside plant cells. Previous work by Perotto et al.[22] identified a glucosamine-containing sphingolipid epitope developmentally regulated in young pea symbiosome membranes, suggesting that GIPCs may play an important role in this process. Consistent with this model, we identified *MtGINT1* as a glycosyltransferase-encoding transcript highly upregulated in the infection and interzone of *M. truncatula* nodules. *MtGINT1* expression was associated with the synthesis of peribacteroid membranes and functioned in HexN(Ac)-GIPC glycosylation *in planta*. Sphingolipidomics further revealed that, although Hex-GIPCs were the predominant sphingolipid in *M. truncatula* roots, HexNAc-GIPCs locally accumulated in nodules and became the dominant species in this tissue. Together, these data illustrate that MtGINT1 functions in local reprogramming of GIPC glycosylation in cells developing peribacteroid membranes.

Our experiments further demonstrated that HexNAc-GIPC glycosylation is required for nodule development and function. Reduction in HexNAc-GIPC content by *MtGINT1* silencing caused strong defects in membrane dynamics in releasing infection threads and symbiosomes. TEM images revealed large amounts of disorganized membrane accumulated at sites of infection thread release, followed by subsequent senescence of elongating bacteroids. Sphingolipids promote membrane ordering and rigidity,[56] which appears to be lacking in *MtGINT1*-silenced nodules. However, these biophysical properties are largely attributed to intercalating interactions between the ceramide lipid moiety and sterols,[56] and it is unclear how sugar residues contribute to this process. *MtGINT1* silencing also disrupted starch distribution at the developmental boundary between the interzone and nitrogen fixation zone. This is particularly interesting considering this boundary segregates the

(O–R) TEM images of RNAi nodules 21 dpi.
(O and P) Releasing infection threads (ITs) in *GUS-RNAi* and *MtGINT1-RNAi* nodules.
(Q and R) Elongated bacteroids at the nitrogen fixation zone boundary of *GUS-RNAi* and *MtGINT1-RNAi* nodules (scale bar represents 1 μm).
Asterisks indicate significant differences determined by Student's t test (*$p < 0.05$; **$p < 0.01$; ***$p < 0.005$) for all experiments. See also Figure S3.

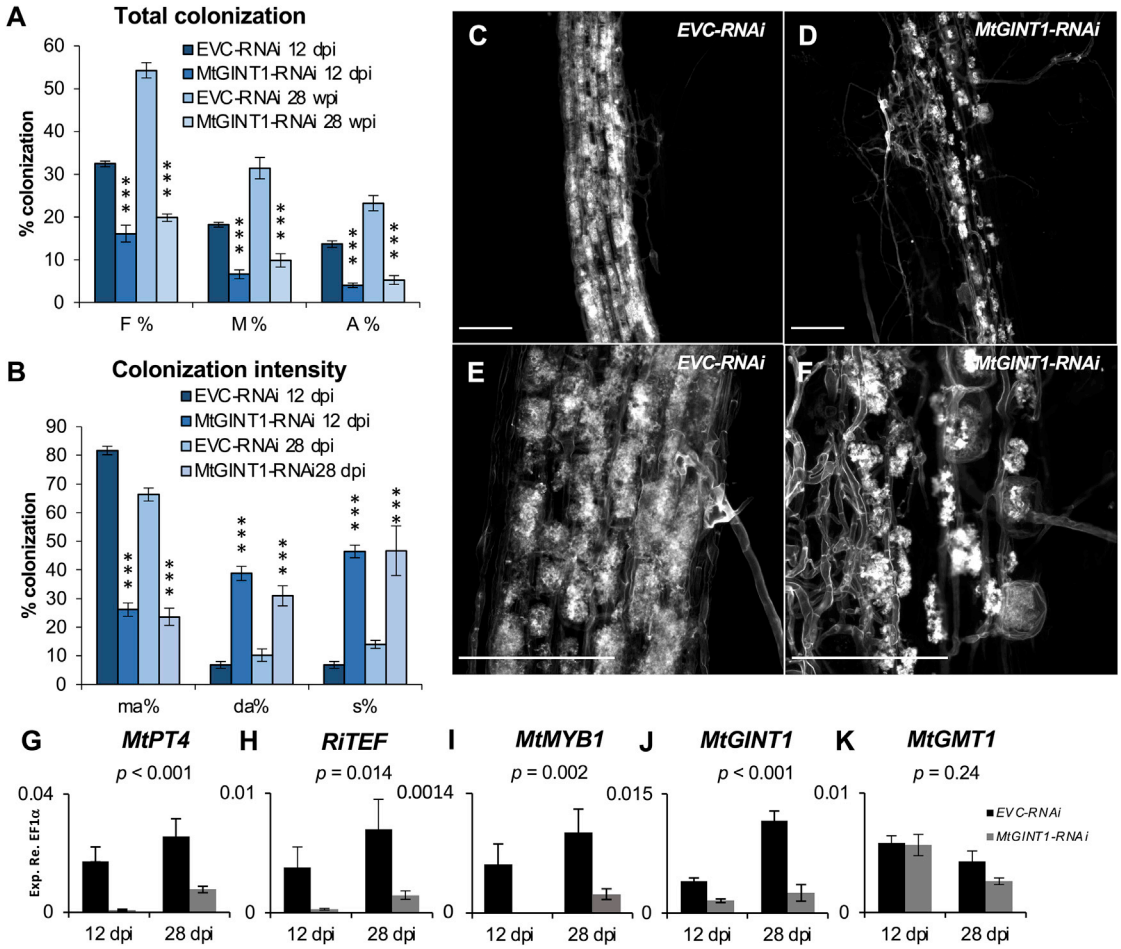

Figure 4. *MtGINT1* silencing impairs mycorrhization and arbuscule development

(A and B) AM colonization quantified by the Trouvelot method at 12 dpi and 28 dpi with *R. irregularis* in roots expressing either *pAtUBQ3:EVC-RNAi* or *pAtUBQ3:MtGINT1-RNAi* constructs; mean ± SEM (n = 5). A%, total arbuscule abundance; da%, density of deformed arbuscules; F%, frequency of infection; ma%, density of mature arbuscules; M%, total mycorrhization; s%, density of fungal septa.

(C–F) Representative images of *EVC-RNAi* and *MtGINT1-RNAi* roots stained with WGA-488 12 dpi with *R. irregularis* (scale bar represents 100 μm).

(G–K) Expression of *MtPT4*, *RiTEF*, *MtMYB1*, *MtGINT1*, and *MtGMT1* relative to *MtEF1-a* measured by qRT-PCR; mean ± SEM (n = 5).

Asterisks indicate significant difference from *EVC-RNAi* control determined by Student's t test (A and B) and two-way ANOVA (G–K; *p < 0.05; **p < 0.01; ***p < 0.005). See also Figure S4.

distribution of GIPCs and galactolipids between young and mature symbiosomes, respectively.[22]

We investigated whether the bacterial cell death observed in *MtGINT1*-silenced nodules was caused by increased SA-mediated defense response. However, both SA content and defense-related gene expression was actually decreased relative to control nodules. We hypothesized this was because *MtGINT1* silencing did not increase the accumulation of bioactive sphingolipid intermediates, like GlcA-IPC and ceramide, known to trigger defense response.[32,36] Therefore, we concluded that the nodulation phenotype associated with *MtGINT1* silencing was not caused by increased defense response and may be more directly attributed to the observed defects in membrane morphology. Loss of membrane organization and integrity may also help explain the increased H_2O_2 detected in the absence of defense response, as membrane redox systems in *M. truncatula* have previously been shown to reside in detergent-insoluble membrane rafts.[57]

MtGINT1 expression was also upregulated in roots colonized by AM fungi. The *MtGINT1* promoter was spatially active in cells that contained arbuscules, which suggested that MtGINT1 may contribute HexN(Ac)-GIPCs to periarbuscular membranes. Activity of the *MtGINT1* promoter was consistent with two previous LCM transcriptomic studies, which support that *MtGINT1* expression is upregulated in arbuscule-containing cells. Furthermore, *MtGINT1* is also a downstream target of arbuscule-specific transcription factor RAM1.[58] RAM1 controls the synthesis and transfer of lipids to AM fungi but may also regulate growth of the periarbuscular membrane itself. *MtGINT1* silencing strongly impaired AM colonization and arbuscule development at 12, 28, and 35 dpi with *R. irregularis*, demonstrating that HexN(Ac)-GIPC glycosylation was functionally important for

AM symbiosis. Arbuscules appeared small and stunted at all time points with an increase in hyphal septation relative to control roots. Expression of *RiTEF* and *MtPT4* was also significantly reduced in *MtGINT1*-silenced roots consistent with observed structures quantified by microscopy. Expression of transcription factor *MtMYB1* was also significantly reduced, which indicated that the observed AM phenotype was not caused by programmed senesce, similar to results obtained from nodulation experiments.

The differential expression pattern of *MtGINT1* and *MtGMT1* in root nodules and AM-colonized roots indicates that local changes in HexNAc-GIPC glycosylation are both a shared and distinguishing feature of cells engaged in symbiosis. Knockdown of *MtGINT1* expression resulted in analogous senescent phenotypes in nodules and AM roots, where endosymbiotic structures were unable to persist inside plant cells. Together, these data demonstrate that HexNAc-GIPC glycosylation is functionally important for symbiosis and imply unique properties for the *N*-acetyl glucosamine glycan decoration. This is supported by our recent study in *A. thaliana*, which has shown that mannose- and glucosamine-decorated GIPC glycans are not functionally interchangeable.[31] Furthermore, the biochemical data presented in this study indicate that reduction in HexN(Ac)-GIPC content upon *MtGINT1* silencing resulted in a relative increase in other glycosphingolipid species, such as Hex-GIPC and GlcCer, but not cytotoxic sphingolipid intermediates, which in part further suggest an important functional role for the HexN(Ac) decoration. The significance of this within the context of symbiosis is not immediately clear but likely reflects important structural, biophysical, or signaling properties. In this regard, it is interesting to note that GlcNAc-containing molecules have prominent roles in symbiosis signaling,[59–62] and the cell surface of bacteria and fungi is rich in GlcNAc-containing polymers.

Development of plant-microbial interfaces requires massive amounts of coordinated lipid synthesis and polar vesicle trafficking to encapsulate the endosymbiont inside plant cells. Based on the disorganized membrane phenotype in *MtGINT1*-silenced nodules, we hypothesize that specific GIPCs may promote membrane ordering and stability during rapid growth. However, functional differences in the carbohydrate stereochemistry of glycolipids, and the influence they impart on membrane dynamics, have not been investigated in depth either *in vitro* or *in vivo*. In general, the structure-related function of glycan sequences is not well understood, and molecular dynamics simulations indicate that even subtle changes in carbohydrate stereochemistry can have profound effects.[63] Similarly, self-assembly of synthetic vesicles with glucopyranose- and galactopyranose-derived single-chain amphiphiles show that differences in carbohydrate stereochemistry can drastically influence membrane shape and bending,[64] yet the underlying physical principles that drive these differences have not been clearly elucidated.

In mammalian cells, changes in cell surface glycosphingolipid glycosylation are markers of cell identity.[65] In this regard, it has been tempting to speculate whether changes in GIPC glycosylation act in a similar capacity during symbiosis. However, we find this unlikely considering other AM symbiotic plants like rice and tobacco exclusively make HexN(Ac)-type GIPC headgroups and tobacco lacks a GMT1 homolog all together. Therefore, the data suggest that reprogramming of GIPC glycosylation in *M. truncatula* is not linked to cell identity but rather reflects important, possibly conserved, functions within perimicrobial membranes necessary for the development and persistence of the endosymbiont inside plant cells.

STAR★METHODS

Detailed methods are provided in the online version of this paper and include the following:

- KEY RESOURCES TABLE
- RESOURCE AVAILABILITY
  - Lead contact
  - Materials availability
  - Data and code availability
- EXPERIMENTAL MODEL AND SUBJECT DETAILS
  - Plant material growth conditions and inoculation
- METHOD DETAILS
  - Root transformation
  - Vector construction
  - Sphingolipidomics
  - Acetylene Reduction Assay
  - Salicylic acid measurements
  - RNA extraction and qRT-PCR
  - Electron microscopy
  - Confocal laser scanning microscopy
  - Light microscopy and histochemistry
- QUANTIFICATION AND STATISTICAL ANALYSIS
  - Phenotyping
  - qRT-PCR
  - Sphingolipidomics

SUPPLEMENTAL INFORMATION

Supplemental information can be found online at https://doi.org/10.1016/j.cub.2021.03.067.

ACKNOWLEDGMENTS

This work conducted by the Joint BioEnergy Institute was supported by the US Department of Energy, Office of Science, Office of Biological and Environmental Research, through contract DE-AC02-05CH11231 between Lawrence Berkeley National Laboratory and the U.S. Department of Energy. Part of the work was supported by an NSF graduate fellowship to W.M.M. (DGE 1106400) and by JSPS KAKENHI to T.I. (17K15411) and M.K.Y. (26292190). We thank Dr. Mi Yeon Lee for assistance with plant growth during experiments. We thank Dr. Sharon Long for gifting the mCherry *S. meliloti* strain. We thank Dr. Maria Harrison for initial advice with hairy root transformation and AM inoculation. We thank Dr. Natalia Requena for advice on AM quantification via the Trouvelot method.

AUTHOR CONTRIBUTIONS

W.M.M., J.C.M., and H.V.S. designed the research. W.M.M., C.C., T.I., M.K.-Y., E.A.R., H.M.-L.W., and V.B. conducted experiments and analyzed data. W.M.M. and H.V.S. wrote the manuscript. All authors discussed results and approved the final manuscript.

DECLARATION OF INTERESTS

The authors declare no competing interests.

CellPress
OPEN ACCESS

Received: November 5, 2019
Revised: December 10, 2020
Accepted: March 19, 2021
Published: April 14, 2021

REFERENCES

1. Pumplin, N., and Harrison, M.J. (2009). Live-cell imaging reveals periarbuscular membrane domains and organelle location in Medicago truncatula roots during arbuscular mycorrhizal symbiosis. Plant Physiol. *151*, 809–819.
2. Catalano, C.M., Lane, W.S., and Sherrier, D.J. (2004). Biochemical characterization of symbiosome membrane proteins from Medicago truncatula root nodules. Electrophoresis *25*, 519–531.
3. Zhang, Q., Blaylock, L.A., and Harrison, M.J. (2010). Two Medicago truncatula half-ABC transporters are essential for arbuscule development in arbuscular mycorrhizal symbiosis. Plant Cell *22*, 1483–1497.
4. Harrison, M.J., Dewbre, G.R., and Liu, J. (2002). A phosphate transporter from Medicago truncatula involved in the acquisition of phosphate released by arbuscular mycorrhizal fungi. Plant Cell *14*, 2413–2429.
5. Guether, M., Neuhäuser, B., Balestrini, R., Dynowski, M., Ludewig, U., and Bonfante, P. (2009). A mycorrhizal-specific ammonium transporter from Lotus japonicus acquires nitrogen released by arbuscular mycorrhizal fungi. Plant Physiol. *150*, 73–83.
6. Vincill, E.D., Szczyglowski, K., and Roberts, D.M. (2005). GmN70 and LjN70. Anion transporters of the symbiosome membrane of nodules with a transport preference for nitrate. Plant Physiol. *137*, 1435–1444.
7. Clarke, V.C., Loughlin, P.C., Day, D.A., and Smith, P.M.C. (2014). Transport processes of the legume symbiosome membrane. Front. Plant Sci. *5*, 699.
8. Bapaume, L., and Reinhardt, D. (2012). How membranes shape plant symbioses: signaling and transport in nodulation and arbuscular mycorrhiza. Front. Plant Sci. *3*, 223.
9. Rich, M.K., Schorderet, M., and Reinhardt, D. (2014). The role of the cell wall compartment in mutualistic symbioses of plants. Front. Plant Sci. *5*, 238.
10. Genre, A., Chabaud, M., Faccio, A., Barker, D.G., and Bonfante, P. (2008). Prepenetration apparatus assembly precedes and predicts the colonization patterns of arbuscular mycorrhizal fungi within the root cortex of both Medicago truncatula and Daucus carota. Plant Cell *20*, 1407–1420.
11. Genre, A., Chabaud, M., Timmers, T., Bonfante, P., and Barker, D.G. (2005). Arbuscular mycorrhizal fungi elicit a novel intracellular apparatus in Medicago truncatula root epidermal cells before infection. Plant Cell *17*, 3489–3499.
12. Fournier, J., Timmers, A.C.J., Sieberer, B.J., Jauneau, A., Chabaud, M., and Barker, D.G. (2008). Mechanism of infection thread elongation in root hairs of Medicago truncatula and dynamic interplay with associated rhizobial colonization. Plant Physiol. *148*, 1985–1995.
13. Genre, A., Ivanov, S., Fendrych, M., Faccio, A., Zársky, V., Bisseling, T., and Bonfante, P. (2012). Multiple exocytotic markers accumulate at the sites of perifungal membrane biogenesis in arbuscular mycorrhizas. Plant Cell Physiol. *53*, 244–255.
14. Ivanov, S., and Harrison, M.J. (2019). Accumulation of phosphoinositides in distinct regions of the periarbuscular membrane. New Phytol. *221*, 2213–2227.
15. Ivanov, S., Fedorova, E.E., Limpens, E., De Mita, S., Genre, A., Bonfante, P., and Bisseling, T. (2012). Rhizobium-legume symbiosis shares an exocytotic pathway required for arbuscule formation. Proc. Natl. Acad. Sci. USA *109*, 8316–8321.
16. Zhang, X., Pumplin, N., Ivanov, S., and Harrison, M.J. (2015). EXO70I is required for development of a sub-domain of the periarbuscular membrane during arbuscular mycorrhizal symbiosis. Curr. Biol. *25*, 2189–2195.
17. Huisman, R., Hontelez, J., Mysore, K.S., Wen, J., Bisseling, T., and Limpens, E. (2016). A symbiosis-dedicated SYNTAXIN OF PLANTS 13II isoform controls the formation of a stable host-microbe interface in symbiosis. New Phytol. *211*, 1338–1351.
18. Bonfante, P. (2001). At the interface between mycorrhizal fungi and plants: the structural organization of cell wall, plasma membrane and cytoskeleton. In Fungal Associations, B. Hock, ed. (Springer Berlin Heidelberg), pp. 45–61.
19. Bonfante-Fasolo, P., Tamagnone, L., Peretto, R., Esquerré-Tugayé, M.T., Mazau, D., Mosiniak, M., and Vian, B. (1991). Immunocytochemical location of hydroxyproline rich glycoproteins at the interface between a mycorrhizal fungus and its host plants. Protoplasma *165*, 127–138.
20. Balestrini, R., Hahn, M.G., Faccio, A., Mendgen, K., and Bonfante, P. (1996). Differential localization of carbohydrate epitopes in plant cell walls in the presence and absence of arbuscular mycorrhizal fungi. Plant Physiol. *111*, 203–213.
21. Perotto, S., Vandenbosch, K.A., Butcher, G.W., and Brewin, N.J. (1991). Molecular composition and development of the plant with the peribacteroid membrane of pea root nodules. Development *112*, 763–773.
22. Perotto, S., Donovan, N., Drobak, B.K., and Brewin, N.J. (1995). Differential expression of a glycosyl inositol phospholipid antigen on the peribacteroid membrane during pea nodule development. Mol. Plant Microbe Interact. *8*, 560–568.
23. Brockerhoff, H. (1963). Breakdown of phospholipids in mild alkaline hydrolysis. J. Lipid Res. *4*, 96–99.
24. Gronnier, J., Germain, V., Gouguet, P., Cacas, J.-L., and Mongrand, S. (2016). GIPC: glycosyl inositol phospho ceramides, the major sphingolipids on earth. Plant Signal. Behav. *11*, e1152438.
25. Cacas, J.-L., Buré, C., Furt, F., Maalouf, J.-P., Badoc, A., Cluzet, S., Schmitter, J.-M., Antajan, E., and Mongrand, S. (2013). Biochemical survey of the polar head of plant glycosylinositolphosphoceramides unravels broad diversity. Phytochemistry *96*, 191–200.
26. Cacas, J.-L., Buré, C., Grosjean, K., Gerbeau-Pissot, P., Lherminier, J., Rombouts, Y., Maes, E., Bossard, C., Gronnier, J., Furt, F., et al. (2016). Revisiting plant plasma membrane lipids in tobacco: a focus on sphingolipids. Plant Physiol. *170*, 367–384.
27. Sperling, P., Franke, S., Lüthje, S., and Heinz, E. (2005). Are glucocerebrosides the predominant sphingolipids in plant plasma membranes? Plant Physiol. Biochem. *43*, 1031–1038.
28. Markham, J.E., Lynch, D.V., Napier, J.A., Dunn, T.M., and Cahoon, E.B. (2013). Plant sphingolipids: function follows form. Curr. Opin. Plant Biol. *16*, 350–357.
29. Cacas, J.-L., Furt, F., Le Guédard, M., Schmitter, J.-M., Buré, C., Gerbeau-Pissot, P., Moreau, P., Bessoule, J.-J., Simon-Plas, F., and Mongrand, S. (2012). Lipids of plant membrane rafts. Prog. Lipid Res. *51*, 272–299.
30. Grosjean, K., Mongrand, S., Beney, L., Simon-Plas, F., and Gerbeau-Pissot, P. (2015). Differential effect of plant lipids on membrane organization: specificities of phytosphingolipids and phytosterols. J. Biol. Chem. *290*, 5810–5825.
31. Ishikawa, T., Fang, L., Rennie, E.A., Sechet, J., Yan, J., Jing, B., Moore, W., Cahoon, E.B., Scheller, H.V., Kawai-Yamada, M., and Mortimer, J.C. (2018). GLUCOSAMINE INOSITOLPHOSPHORYLCERAMIDE TRANSFERASE1 (GINT1) is a GlcNAc-containing glycosylinositol phosphorylceramide glycosyltransferase. Plant Physiol. *177*, 938–952.
32. Fang, L., Ishikawa, T., Rennie, E.A., Murawska, G.M., Lao, J., Yan, J., Tsai, A.Y.-L., Baidoo, E.E.K., Xu, J., Keasling, J.D., et al. (2016). Loss of inositol phosphorylceramide sphingolipid mannosylation induces plant immune responses and reduces cellulose content in Arabidopsis. Plant Cell *28*, 2991–3004.
33. Mortimer, J.C., and Scheller, H.V. (2020). Synthesis and function of complex sphingolipid glycosylation. Trends Plant Sci. *25*, 522–524.
34. Singh, S.K., Eland, C., Harholt, J., Scheller, H.V., and Marchant, A. (2005). Cell adhesion in Arabidopsis thaliana is mediated by ECTOPICALLY PARTING CELLS 1–a glycosyltransferase (GT64) related to the animal exostosins. Plant J. *43*, 384–397.

35. Rennie, E.A., Ebert, B., Miles, G.P., Cahoon, R.E., Christiansen, K.M., Stonebloom, S., Khatab, H., Twell, D., Petzold, C.J., Adams, P.D., et al. (2014). Identification of a sphingolipid α-glucuronosyltransferase that is essential for pollen function in Arabidopsis. Plant Cell *26*, 3314–3325.

36. Tartaglio, V., Rennie, E.A., Cahoon, R., Wang, G., Baidoo, E., Mortimer, J.C., Cahoon, E.B., and Scheller, H.V. (2017). Glycosylation of inositol phosphorylceramide sphingolipids is required for normal growth and reproduction in Arabidopsis. Plant J. *89*, 278–290.

37. Lenarčič, T., Albert, I., Böhm, H., Hodnik, V., Pirc, K., Zavec, A.B., Podobnik, M., Pahovnik, D., Žagar, E., Pruitt, R., et al. (2017). Eudicot plant-specific sphingolipids determine host selectivity of microbial NLP cytolysins. Science *358*, 1431–1434.

38. Roux, B., Rodde, N., Jardinaud, M.-F., Timmers, T., Sauviac, L., Cottret, L., Carrère, S., Sallet, E., Courcelle, E., Moreau, S., et al. (2014). An integrated analysis of plant and bacterial gene expression in symbiotic root nodules using laser-capture microdissection coupled to RNA sequencing. Plant J. *77*, 817–837.

39. Hogekamp, C., and Küster, H. (2013). A roadmap of cell-type specific gene expression during sequential stages of the arbuscular mycorrhiza symbiosis. BMC Genomics *14*, 306.

40. Gaude, N., Bortfeld, S., Duensing, N., Lohse, M., and Krajinski, F. (2012). Arbuscule-containing and non-colonized cortical cells of mycorrhizal roots undergo extensive and specific reprogramming during arbuscular mycorrhizal development. Plant J. *69*, 510–528.

41. Cantarel, B.L., Coutinho, P.M., Rancurel, C., Bernard, T., Lombard, V., and Henrissat, B. (2009). The Carbohydrate-Active EnZymes database (CAZy): an expert resource for Glycogenomics. Nucleic Acids Res. *37*, D233–D238.

42. Ivanov, S., and Harrison, M.J. (2014). A set of fluorescent protein-based markers expressed from constitutive and arbuscular mycorrhiza-inducible promoters to label organelles, membranes and cytoskeletal elements in Medicago truncatula. Plant J. *80*, 1151–1163.

43. Grebenok, R.J., Lambert, G.M., and Galbraith, D.W. (1997). Characterization of the targeted nuclear accumulation of GFP within the cells of transgenic plants. Plant J. *12*, 685–696.

44. Sridharan, G., and Shankar, A.A. (2012). Toluidine blue: a review of its chemistry and clinical utility. J. Oral Maxillofac. Pathol. *16*, 251–255.

45. Mortimer, J.C., Yu, X., Albrecht, S., Sicilia, F., Huichalaf, M., Ampuero, D., Michaelson, L.V., Murphy, A.M., Matsunaga, T., Kurz, S., et al. (2013). Abnormal glycosphingolipid mannosylation triggers salicylic acid-mediated responses in Arabidopsis. Plant Cell *25*, 1881–1894.

46. Ternes, P., Feussner, K., Werner, S., Lerche, J., Iven, T., Heilmann, I., Riezman, H., and Feussner, I. (2011). Disruption of the ceramide synthase LOH1 causes spontaneous cell death in Arabidopsis thaliana. New Phytol. *192*, 841–854.

47. Brodersen, P., Petersen, M., Pike, H.M., Olszak, B., Skov, S., Odum, N., Jørgensen, L.B., Brown, R.E., and Mundy, J. (2002). Knockout of Arabidopsis accelerated-cell-death11 encoding a sphingosine transfer protein causes activation of programmed cell death and defense. Genes Dev. *16*, 490–502.

48. Magnin-Robert, M., Le Bourse, D., Markham, J., Dorey, S., Clément, C., Baillieul, F., and Dhondt-Cordelier, S. (2015). Modifications of sphingolipid content affect tolerance to hemibiotrophic and necrotrophic pathogens by modulating plant defense responses in Arabidopsis. Plant Physiol. *169*, 2255–2274.

49. Shi, C., Yin, J., Liu, Z., Wu, J.-X., Zhao, Q., Ren, J., and Yao, N. (2015). A systematic simulation of the effect of salicylic acid on sphingolipid metabolism. Front. Plant Sci. *6*, 186.

50. Berkey, R., Bendigeri, D., and Xiao, S. (2012). Sphingolipids and plant defense/disease: the "death" connection and beyond. Front. Plant Sci. *3*, 68.

51. Wang, C., Yu, H., Luo, L., Duan, L., Cai, L., He, X., Wen, J., Mysore, K.S., Li, G., Xiao, A., et al. (2016). NODULES WITH ACTIVATED DEFENSE 1 is required for maintenance of rhizobial endosymbiosis in Medicago truncatula. New Phytol. *212*, 176–191.

52. Horváth, B., Domonkos, Á., Kereszt, A., Szűcs, A., Ábrahám, E., Ayaydin, F., Bóka, K., Chen, Y., Chen, R., Murray, J.D., et al. (2015). Loss of the nodule-specific cysteine rich peptide, NCR169, abolishes symbiotic nitrogen fixation in the Medicago truncatula dnf7 mutant. Proc. Natl. Acad. Sci. USA *112*, 15232–15237.

53. Kim, M., Chen, Y., Xi, J., Waters, C., Chen, R., and Wang, D. (2015). An antimicrobial peptide essential for bacterial survival in the nitrogen-fixing symbiosis. Proc. Natl. Acad. Sci. USA *112*, 15238–15243.

54. Heck, C., Kuhn, H., Heidt, S., Walter, S., Rieger, N., and Requena, N. (2016). Symbiotic fungi control plant root cortex development through the novel GRAS transcription factor MIG1. Curr. Biol. *26*, 2770–2778.

55. Floss, D.S., Gomez, S.K., Park, H.-J., MacLean, A.M., Müller, L.M., Bhattarai, K.K., Lévesque-Tremblay, V., Maldonado-Mendoza, I.E., and Harrison, M.J. (2017). A transcriptional program for arbuscule degeneration during AM symbiosis is regulated by MYB1. Curr. Biol. *27*, 1206–1212.

56. Ramstedt, B., and Slotte, J.P. (2006). Sphingolipids and the formation of sterol-enriched ordered membrane domains. Biochim. Biophys. Acta *1758*, 1945–1956.

57. Lefebvre, B., Furt, F., Hartmann, M.-A., Michaelson, L.V., Carde, J.-P., Sargueil-Boiron, F., Rossignol, M., Napier, J.A., Cullimore, J., Bessoule, J.-J., and Mongrand, S. (2007). Characterization of lipid rafts from Medicago truncatula root plasma membranes: a proteomic study reveals the presence of a raft-associated redox system. Plant Physiol. *144*, 402–418.

58. Luginbuehl, L.H., Menard, G.N., Kurup, S., Van Erp, H., Radhakrishnan, G.V., Breakspear, A., Oldroyd, G.E.D., and Eastmond, P.J. (2017). Fatty acids in arbuscular mycorrhizal fungi are synthesized by the host plant. Science *356*, 1175–1178.

59. Genre, A., Chabaud, M., Balzergue, C., Puech-Pagès, V., Novero, M., Rey, T., Fournier, J., Rochange, S., Bécard, G., Bonfante, P., and Barker, D.G. (2013). Short-chain chitin oligomers from arbuscular mycorrhizal fungi trigger nuclear Ca2+ spiking in Medicago truncatula roots and their production is enhanced by strigolactone. New Phytol. *198*, 190–202.

60. Ehrhardt, D.W., Wais, R., and Long, S.R. (1996). Calcium spiking in plant root hairs responding to Rhizobium nodulation signals. Cell *85*, 673–681.

61. Nadal, M., Sawers, R., Naseem, S., Bassin, B., Kulicke, C., Sharman, A., An, G., An, K., Ahern, K.R., Romag, A., et al. (2017). An N-acetylglucosamine transporter required for arbuscular mycorrhizal symbioses in rice and maize. Nat. Plants *3*, 17073.

62. Wong, J.E.M.M., Gysel, K., Birkefeldt, T.G., Vinther, M., Muszyński, A., Azadi, P., Laursen, N.S., Sullivan, J.T., Ronson, C.W., Stougaard, J., and Andersen, K.R. (2020). Structural signatures in EPR3 define a unique class of plant carbohydrate receptors. Nat. Commun. *11*, 3797.

63. Fogarty, C.A., Harbison, A.M., Dugdale, A.R., and Fadda, E. (2020). How and why plants and human N-glycans are different: insight from molecular dynamics into the "glycoblocks" architecture of complex carbohydrates. bioRxiv. https://doi.org/10.1101/2020.05.22.110528.

64. Bhattacharya, A., Brea, R.J., Song, J.-J., Bhattacharya, R., Sinha, S.K., and Devaraj, N.K. (2019). Single-chain β-d-glycopyranosylamides of unsaturated fatty acids: self-assembly properties and applications to artificial cell development. J. Phys. Chem. B *123*, 3711–3720.

65. Russo, D., Capolupo, L., Loomba, J.S., Sticco, L., and D'Angelo, G. (2018). Glycosphingolipid metabolism in cell fate specification. J. Cell Sci. *131*, jcs219204.

66. Devers, E.A., Teply, J., Reinert, A., Gaude, N., and Krajinski, F. (2013). An endogenous artificial microRNA system for unraveling the function of root endosymbioses related genes in Medicago truncatula. BMC Plant Biol. *13*, 82.

67. Floss, D.S., Schmitz, A.M., Starker, C.G., Gantt, J.S., and Harrison, M.J. (2013). Gene silencing in Medicago truncatula roots using RNAi. Methods Mol. Biol. *1069*, 163–177.

68. Yan, P., Shen, W., Gao, X., Li, X., Zhou, P., and Duan, J. (2012). High-throughput construction of intron-containing hairpin RNA vectors for RNAi in plants. PLoS ONE *7*, e38186.

69. Nakagawa, T., Kurose, T., Hino, T., Tanaka, K., Kawamukai, M., Niwa, Y., Toyooka, K., Matsuoka, K., Jinbo, T., and Kimura, T. (2007). Development of series of gateway binary vectors, pGWBs, for realizing efficient construction of fusion genes for plant transformation. J. Biosci. Bioeng. *104*, 34–41.

70. Ishikawa, T., Ito, Y., and Kawai-Yamada, M. (2016). Molecular characterization and targeted quantitative profiling of the sphingolipidome in rice. Plant J. *88*, 681–693.

71. Eudes, A., Juminaga, D., Baidoo, E.E.K., Collins, F.W., Keasling, J.D., and Loqué, D. (2013). Production of hydroxycinnamoyl anthranilates from glucose in Escherichia coli. Microb. Cell Fact. *12*, 62.

72. Wielopolska, A., Townley, H., Moore, I., Waterhouse, P., and Helliwell, C. (2005). A high-throughput inducible RNAi vector for plants. Plant Biotechnol. J. *3*, 583–590.

73. Gianinazzi-Pearson, V., Gianin Trouvelot, A., Kough, J.L., and Gianinazzi-Pearson, V. (1986). Mesure du taux de mycorhization VA d'un système radiculaire. Recherche de méthodes d'estimation ayant une signification fonctionnelle. In Physiological and Genetical Aspects of Mycorrhizae, V. Gianinazzi-Pearson, and S. Gianinazzi, eds. (INRA), pp. 217–221.

STAR★METHODS

KEY RESOURCES TABLE

REAGENT or RESOURCE	SOURCE	IDENTIFIER
Bacterial and virus strains		
Sinorhizobium meliloti stain Rm1021	ATCC	ATCC51124
Sinorhizobium meliloti strain Rm1201 mCherry	Devers et al.[66]	N/A
Agrobacteria rhizogenes strain ARqua1	Maria Harrison Floss et al.[67]	N/A
Chemicals, peptides, and recombinant proteins		
Half strength Murashige and Skoog basal salt media without nitrogen	Phytotechlab	M531
Half strength modified Hoagland's basal salt mixture	Yan et al.[68]	N/A
TRIzol reagent	Thermo-Fischer	15596-026
TURBO DNA-free kit	Thermo-Fischer	AM1907
RNEAsy purification column	QIAGEN	74907
qRT-PCR cDNA synthesis kit	Biorad	1708840
Power Up syber green qPCR master mix	Thermo-Fischer	A25642
Acetylene	Airgas	AC B
Ethylene	Supelco	25881-U
Wheat Germ Alexafluor 488	Thermo-Fischer	W11261
Propidium iodide	Thermo-Fischer	P1304MP
Syto 9	Thermo-Fischer	S34854
Lugol reagent	Sigma-Aldrich	L-6146
Toluidine Blue-O	Sigma-Aldrich	198161
5-Bromo-4-chloro-3-indolyl β-glucuronide cyclohexamine salt	Sigma-Aldrich	B8049
3,3-diaminobenzidine	Alfa Aesar	H54000
Technovit 7100	Electron Microscopy Science	14653
Epon	Electron Microscopy Science	N/A
Glutaraldehyde	Electron Microscopy Science	16000
Sodium cacodylate buffer	Electron Microscopy Science	11650
Experimental models: organisms/strains		
Medicago truncatula cv jemalong ecotype A17	Noble Foundation	N/A
Arabidopsis thaliana ecotype Col-0	ABRC	N/A
Rhizophagus irregularis DAOM 181602	PremierTech	N/A
Oligonucleotides		
All primer sequences are listed in Table S1	N/A	N/A
Recombinant DNA		
pHELLSGATE12	CSIRO	N/A
pGWB1, pGWB3, pGWB17, pGWB40	Nakagawa et al.[69]	N/A
pRed	Ishikawa et al.[70]	N/A
pRedRNAi	Ishikawa et al.[70]	N/A
pRNAi-GG	Eudes et al.[71]	N/A
Software and algorithms		
Medicago Gene Expression Atlas	https://mtgea.noble.org/v3/	N/A
Symbimics database	https://lant.toulouse.inra.fr//symbimics/	N/A

RESOURCE AVAILABILITY

Lead contact

Further information and requests for resources and reagents should be directed to and will be fulfilled by the Lead Contact, Henrik V. Scheller (hscheller@lbl.gov).

Materials availability

This study did not generate new unique reagents. Plasmids will be made available upon request.

Data and code availability

Source data for figures in the paper is available upon request.

EXPERIMENTAL MODEL AND SUBJECT DETAILS

Plant material growth conditions and inoculation

Medicago truncatula Gaertn, cv Jemalong A17 was used for all experiments in this study. Plants were grown in controlled growth chambers at 22°C, under 16 h photoperiod, with 300 μmol m^{-2} s^{-1} light intensity. All plants were grown in washed autoclaved sand packed in plastic cones (l = 21 cm, d = 4cm). Plants were watered daily and fertilized twice a week with either half-strength Murishage and Skoog (MS) medium for general growth experiments, MS medium without nitrogen for nodulation experiments, or half-strength Hoagland's medium modified with 20 μM phosphate for AM experiments. For nodulation experiments plants were flood inoculated with 5 mL of bacterial suspension (0.1 OD600) in water. In AM experiments plants were inoculated with approximately 1200 spores applied directly to the root system. Sterile *Rhizophagus irregularis* (DAOM 181602) spores were purchased from Premier Tech (Rivière-du-Loup, Québec, Canada).

METHOD DETAILS

Root transformation

Seeds were scarified in concentrated sulfuric acid for 10 min, washed, surface sterilized with 10% (v/v) bleach solution, washed, and imbibed in distilled H_2O for 2 h. Imbibed seeds were placed in Petri dishes containing 1% (w/v) water agar and stratified for 26 h at 4°C. Seeds were then germinated at 25°C on inverted plates for 18h to enable gravitropic bending of the radicle, except for the qRT-PCR experiments in Figures 1C and 1D, where seeds were germinated directly in sand cones after scarification and stratification. Emerging radicles were cut with sterile scalpel, dragged across a bacterial lawn of *Agrobacterium rhizogenes* ARqua1[67] containing the appropriate construct, and placed on slanted Fahraeus medium containing 25 mg/mL kanamycin. Transgenic root systems were allowed to develop for 14 d in a growth chamber at 18°C. Plantlets containing transgenic root systems were transferred to sterile washed sand packed in plastic cone containers and allowed to recover for one week prior to inoculation. Root transformation methods and bacterial culture methods have previously been described in detail.[67]

Vector construction

MtGINT1-RNAi constructs targeted a 400-base pair region beginning at the translational start site of the *MtGINT1* coding sequence, which was determined to be gene-specific by BLAST search against the *M. truncatula* genome. The sequence was cloned into the Gateway entry vector pENTR1A (Thermo Fisher Scientific) using XbaI/XhoI restriction sites and recombined into pHELLSGATE12 RNAi vector (CSIRO) by LR reaction.[72] A 423 bp sequence targeting the *E. coli* β-glucuronidase gene (GUS) was used as a control. RNAi constructs with the same target sequences were also generated in the pRNAi-GG and pRed-RNAi vectors by restriction cloning.[66,68] All nodulation experiments used the *35 s* driven pHELLSGATE12 RNAi vector. Mycorrhizal experiments used both the pHELLSGATE12 and *AtUBQ3* driven pRed-RNAi vectors with similar results. Sphingolipidomic experiments used the *35 s* driven pRNAi-GG vector in uninoculated roots and pRed-RNAi vector in dissected nodules. In all cases the same 400-bp *MtGINT1* target sequence was used for silencing and produced similar results. For *MtGINT1* promoter reporter constructs 2 kb of genomic sequence upstream of the start codon was TOPO cloned into GateWay entry vector pCR8 (Thermo Fisher Scientific) and recombined into pGWB3 and pGWB40 by LR reaction for GUS and YFP expression, respectively.[69] For BCP1-mCherry reporter constructs, 3 kb of *MtGINT1* genomic sequence was recombined with the BCP1-mCherry coding sequence[42] into pCR8 by In-Fusion cloning (Takara Bio Science) and transferred into pGWB1 by LR reaction. For overexpression of *MtGINT1* in *M. truncatula* roots, the full-length *MtGINT1* coding sequence was cloned directly into pRed using SpeI and MluI restriction sites to generate *AtUBQ3:MtGINT1*.[66] For heterologous expression of *MtGINT1* in *A. thaliana*, the coding sequence without stop codon was TOPO cloned into pCR8 and recombined into pGWB17[69] by LR reaction. All constructs were confirmed by sequencing and primers used for PCR and cloning are listed in Table S1.

Sphingolipidomics

Lyophilized plant tissues (5 to 10 mg) were homogenized in 450 μl of methanol/1-butanol (1:2, v/v) and subjected to heat-denaturation of enzymes at 80°C for 10 min. The homogenate was mixed with 300 μl of 1 N KOH and further incubated at 60°C for 30 min to

eliminate glycerolipids. The mixture was acidified with 1.5 mL of 0.4 N HCl and vigorously mixed with additional 1 mL 1-butanol by vortexing for 30 s. After centrifugation (10,000 x *g*, 5 min, room temperature) for phase separation, the upper 1-butanol layer was collected and evaporated. The residue was dissolved in 150 μl of tetrahydrofuran/methanol/water (2:1:2, v/v/v) containing 0.1% (v/v) formic acid. GIPC composition was analyzed by LC-MS/MS according to previous reports.[32,70]

Acetylene Reduction Assay

Nitrogen fixation was measured by acetylene reduction assay in silenced roots at 14 and 28 dpi with *S. meliloti*. Chimeric plants were gently uprooted from sand and placed on a strip of Whatman filter paper (pre-wet with half-strength MS without nitrogen) inside a 25 mL culture tube topped with a rubber septum. Acetylene (1 mL) was extracted from a Tedlar gas bag (Supelco) with a 1 mL syringe fitted with an air-tight Swagelok stopper and injected into the culture tube. Culture tubes were then placed in a plant growth chamber for 6 h prior to sampling. Gas samples were extracted from tubes with a 10 mL syringe, as above, and measured using gas chromatography flame ionization detection on a Shimadzu GC-2014 with HayeSep N column.

Salicylic acid measurements

For active SA quantification, 500 mg root tissue was ground in liquid nitrogen and mixed with 1 mL 80% (v/v) methanol and heated at 70°C for 15 minutes. This was repeated four times and pooled methanol exacts were filtered through Amicon Ultra centrifugal filters (10,000 Da MW cutoff, Millipore, Billerica, MA). The filtrate was partitioned with ethyl acetate three times and pooled. Ethyl acetate fractions were dried in speedvac, and resuspended in 50% (v/v) methanol. SA was quantified using HPLC-electrospray ionization (ESI)-time-of-flight (TOF) MS. Detailed running methods are previously described. Acid hydrolysis was omitted to measure active SA within the greater pool of SA-glucoside. Detailed running conditions have previously been described.[71]

RNA extraction and qRT-PCR

Total RNA was extracted using Trizol (Thermo Fisher), treated with Turbo DNaseI (Thermo Fisher), and further purified using an RNEAsy column (QIAGEN). cDNA was prepared using iScript cDNA qRT-PCR synthesis kit (Bio-Rad) from 500 ng of total RNA and diluted 1:4 in nuclease-free water. *MtGINT1* qRT-PCR primers were designed to span the junction between the third and fourth exon outside the RNAi-targeted region of the *MtGINT1* transcript. PowerUp Sybr Green Master Mix (Thermo-Fischer) was used as qRT-PCR reagent and results were collected on CFX-396 qRT-PCR machine (Bio-Rad) for 30 cycles using a 58°C annealing temperature and 200 nM primer concentration. Amplification of all target genes was assessed by melt curve and gene expression was quantified using the $\Delta\Delta C_T$ method relative to the housekeeping gene *MtEF-1α*. All primers are listed in Table S1.

Electron microscopy

Nodules were harvested directly into 0.1 M cacodylate buffer (pH 7.2) containing 2% (v/v) EM-grade glutaraldehyde, with gentle pulling under vacuum for 2 min. Nodules remained in fixation buffer overnight at 4°C and were bisected longitudinally to aid resin infiltration. Nodules were rinsed three times with 0.1 M cacodylate buffer (pH 7.2), stained for 1 h with 1% (w/v) osmium tetraoxide, and rinsed three times with buffer, followed by an additional 3 rinses with distilled water. Seeds were then dehydrated in an acetone gradient (35/50/70/80/95/100/100% v/v) and infiltrated in acetone and epon resin at 2:1, 1:1, and 1:2 dilution ratios for 1 h each, followed by pure epon that was freshly changed after one hour and allowed to infiltrate overnight with gentle rocking. Samples were then infiltrated with pure resin plus accelerator for two hours and embedded in Pelco molds, which were left in a 65°C oven to polymerize for two days. Ultra-thin 70 nm thick sections were collected on to grids using a diamond knife and Reichert microtome. Grids were stained with 2% (v/v) aqueous uranyl acetate for 5 min, rinsed with distilled water five times, stained with lead citrate for 5 min, and rinsed another five times with distilled water using a Pelco Grid Staining System. Grids were imaged using a Technai 1200 electron microscope. For consistency we analyzed two grids per nodule, using at least three nodules per construct.

Confocal laser scanning microscopy

All confocal microscopy was conducted on a Zeiss LSM 710 laser-scanning microscope (Carl Zeiss, Oberkochen, Germany). Live cell imaging of root nodules was observed *S. meliloti* strain expressing mCherry counter stained with 1 mM Calcofluor White to stain plant cell walls. Wild-type *S. meliloti* 1021 was used for live/dead staining of nodules with 5 μM Syto 9 and 30 μM propidium iodide for 20 min at room temperature. In both cases fresh nodule hand sections were made and immediately imaged. Mycorrhizal roots colonized by *R. irregularis* were visualized by staining fungal chitin with 0.5 μg/ml wheat germ agglutinin (WGA) Alexa Fluor 488 (Thermo Fischer Scientific) in 80 μM PIPES buffer (pH 7.0). Mycorrhized roots were fixed in 50% (v/v) ethanol, cleared in 20% (w/v) KOH at 65°C for two days, neutralized, and stained with WGA-488 for at least 3 days at 4°C prior to imaging.

Light microscopy and histochemistry

Images from histochemical staining and fluorescent *MtGINT1* promoter-reporter experiments were acquired on a Leica DM6B microscope equipped with a Leica Hamatsu fluoresce camera and DMC4500 color camera (Leica Microsystems, Buffalo Grove, IL USA). Sectioned nodules were embedded in Technovit 7100 plastic resin (Kulzer Technique, Wehrheim, Germany) according to the manufacturers directions and stained with 0.2% toluidine blue O (TBO) for 60 s prior to viewing. Histochemical detection of H_2O_2 in 3-week-old nodules was performed using 1 mg/mL 3,3-diaminobenzidine (DAB) in buffer (100 mM HEPES-KOH, pH 6.8). Staining was conducted for 6 h in dark, followed by clearing in 95% ethanol, hand sectioning, and imaging.[32,36,51] Starch was

detected by staining fresh nodules with Lugol reagent for 5 min followed by hand sectioning. For GUS staining, root tissues were harvested directly into ice cold 90% acetone and fixed for 30 min, followed by buffer (50mM PO4 buffer, 0.2% Triton X-100, 2mM Ferro/Ferri cyanide) gently infiltrated under vacuum for 30 min. Samples were then placed in buffer containing 2mM X-GLUC and incubated at 37°C overnight. Samples were dehydrated in an ethanol gradient (20/35/50%), fixed with FAA (50% ethanol, 5% acetic acid, 3.7% formaldehyde), and stored in 70% ethanol at 4°C prior to imaging.

QUANTIFICATION AND STATISTICAL ANALYSIS

Phenotyping

Macro phenotypes of RNAi nodules from twelve biological replicates were observed under a stereomicroscope and scored based on the visual presence of leghomglobin. Nitrogen fixation efficiency based on acetylene reduction assay was measured by GC-FID and calculated as the rate of ethylene production (nmol/h) using five biological replicates at 14 dpi and three biological replicates at 21 dpi. AM colonization in RNAi roots at 12 and 28 dpi was quantified using the Trouvelot method[73] by observing WGA-488 stained roots on a Leica DM6B fluorescence microscope. AM root colonization was also quantified by gridline intersect at 35 dpi in a separate experiment and produced similar results. Five biological replicates were used in all AM experiments (n, indicated in figure legends). All bar graph values reflect the mean ± SEM. Microsoft Excel v16 for Mac was used for generating graphs and for Student's t tests (*$p < 0.05$, **$p < 0.01$, ***$p < 0.005$). Results of statistical analyses are shown in the figures.

qRT-PCR

Expression values of at least three biological replicates and three technical replicates were analyzed using the $\Delta\Delta C_T$ method relative to house keeping *MtEF1*α. Three biological replicates were used for surveying *MtGINT1* and *MtGMT1* expression in response to nutrient deficiency and inoculation. Four biological replicates were used in nodulation RNAi experiments and five biological replicates were used for AM RNAi experiments (n, indicated in figure legends). Bar graph values reflect mean values ± SEM. Microsoft Excel v16 for Mac was used for generating graphs and for Student's t tests (*$p < 0.05$, **$p < 0.01$, ***$p < 0.005$) in root survey and nodulation RNAi experiments. Statistical significance in AM RNAi experiments was determined by two-way ANOVA using SPSS Statistics v2.7 (IBM). Results of statistical analyses are shown in the figures.

Sphingolipidomics

Sphingolipidomic survey of root tissues was analyzed using at least three biological replicates and calculated as nmol/g dry weight. Sphingolipid composition of RNAi nodules was analyzed using at least three biological replicates and presented as mol% normalized to total sphingolipid content to correct for size discrepancies between *MtGINT1-RNAi* and *GUS-RNAi* nodules. Sphingolipid content of uninoculated *MtGINT1-RNAi*, *MtGINT1-OE*, and corresponding controls were analyzed using at least four biological replicates and calculated as nmol/g dry weight. The number of replicates is indicated in the figure legends (n). Microsoft Excel v16 for Mac was used for generating graphs and for Student's t tests (*$p < 0.05$, **$p < 0.01$, ***$p < 0.005$). Bar graph values represent mean values ± SEM. Results of statistical analyses are shown in the figures.

Current Biology, Volume *31*

Supplemental Information

Reprogramming sphingolipid glycosylation is required for endosymbiont persistence in *Medicago truncatula*

William M. Moore, Candace Chan, Toshiki Ishikawa, Emilie A. Rennie, Heidi M.-L. Wipf, Veronica Benites, Maki Kawai-Yamada, Jenny C. Mortimer, and Henrik V. Scheller

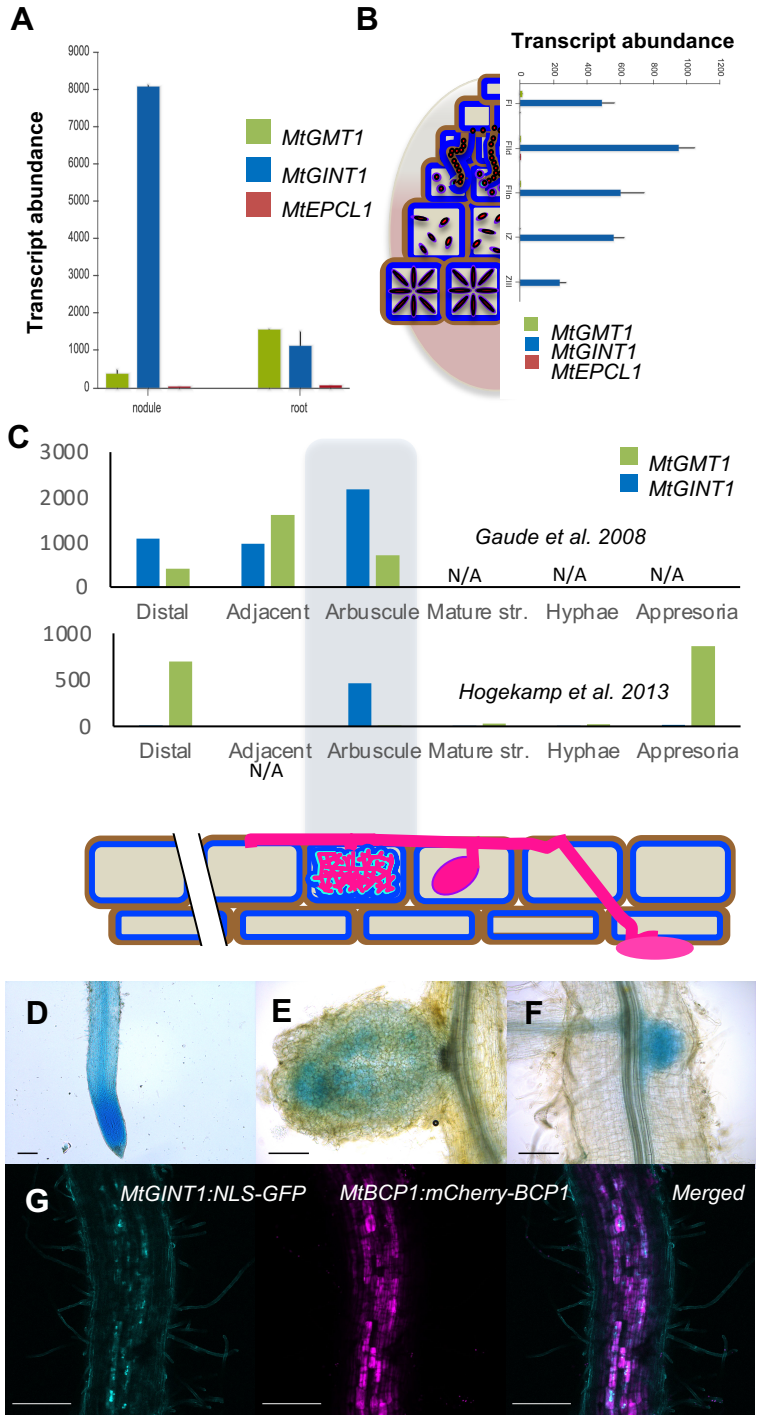

Figure S1. Spatial expression patter of *MtGINT1* and GT family 64 enzymes in *M. truncatula* roots, related to Figure 1C-1H. **(A and B)** Symbimics Database and **(C)** the Medicago Gene Expression Atlas. **(A)** Deseq-normalized RNA-seq reads in root nodules vs roots and **(B)** different nodule developmental zones collected by laser-capture microdissection (FI, meristem; FIId-FIIp, distal and proximal infection zone; IZ, interzone; ZIII, nitrogen fixation zone). Error bars reflect ± SD, n =3. **(C)** Microarray data from different root cell types colonized by *R. irregularis* collected by laser capture microdissection (10, 11). Expression in arbuscule-containing cells is highlighted. Mtr.43583.1.S1_at was used as the *MtGINT1* probe in the Medicago Gene Expression Atlas. **(D-F)** GUS staining of uninoculated **(D)** and nodulated root systems 21 dpi **(E and F)** expressing *pMtGINT1:GUS* in hairy roots. **(G)** Co-expression of *pMtGINT1:NLS-GFP* and *MtBCP1:mCherry-BCP1* in roots colonized by *R. irregularis* 21 dpi imaged by CLSM.

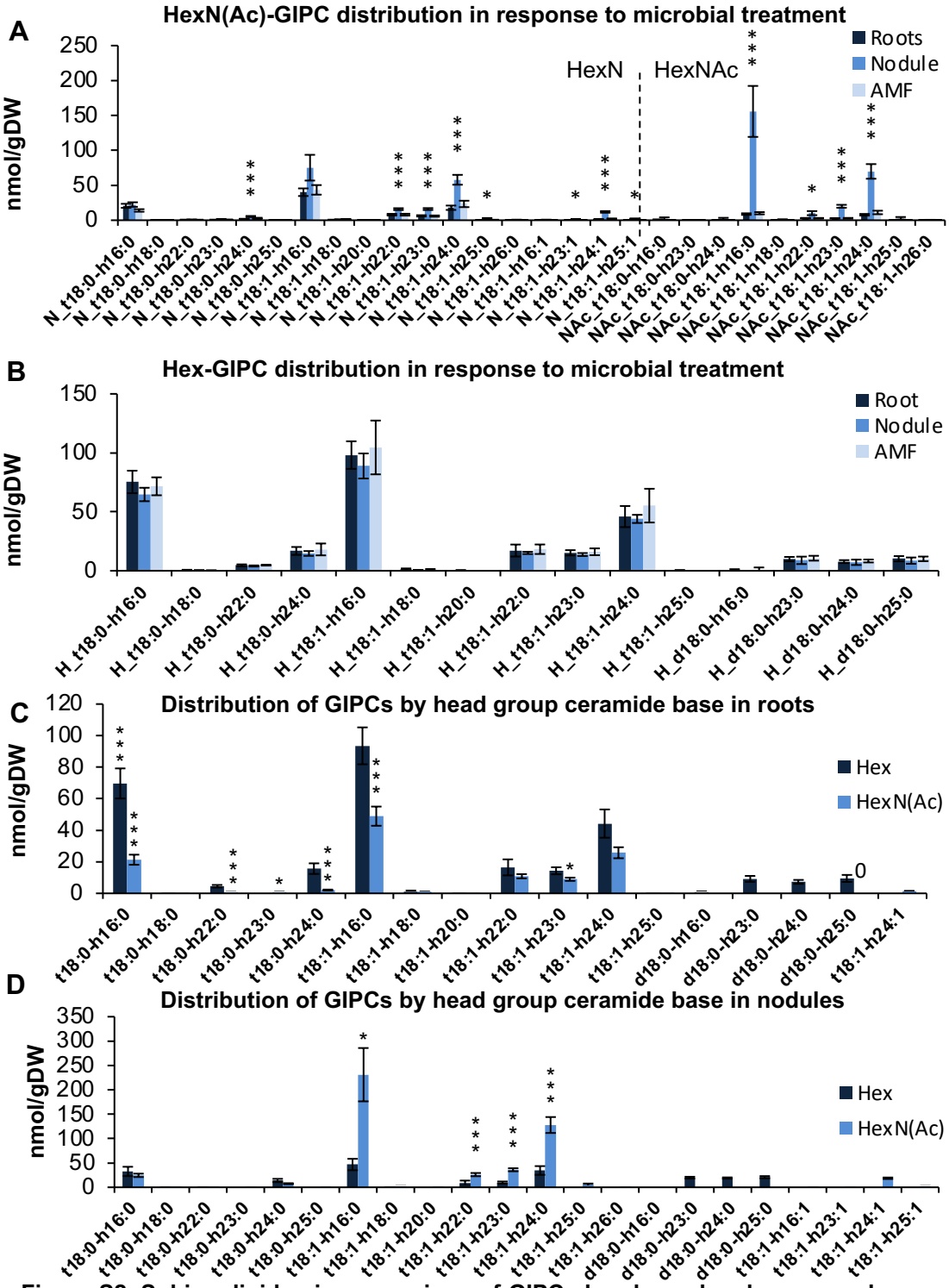

Figure S2. Sphingolipidomic comparison of GIPCs by glycan head group and ceramide base in response to microbial treatment, related to Figure 1J. (A) Response of HexN(Ac)-GIPC and **(B)** Hex-GIPC, by ceramide base, to microbial treatment. Results show that ceramide base usage does not change in response to microbial treatment. HexNAc_t18:1-h16:0 is the dominant GIPC in nodule tissue. **(C)** Comparison between HexN(Ac)-GIPC and Hex-GIPC, by ceramide base in root tissue. **(D)** Comparison between HexN(Ac)-GIPC and Hex-GIPC, by ceramide base in root nodules. Asterisks indicate statistical significance determined by Student's t-test, (p-value: *< 0.05, **<0.01, ***<0.005). Error bars reflect ± SEM (*n*=5).

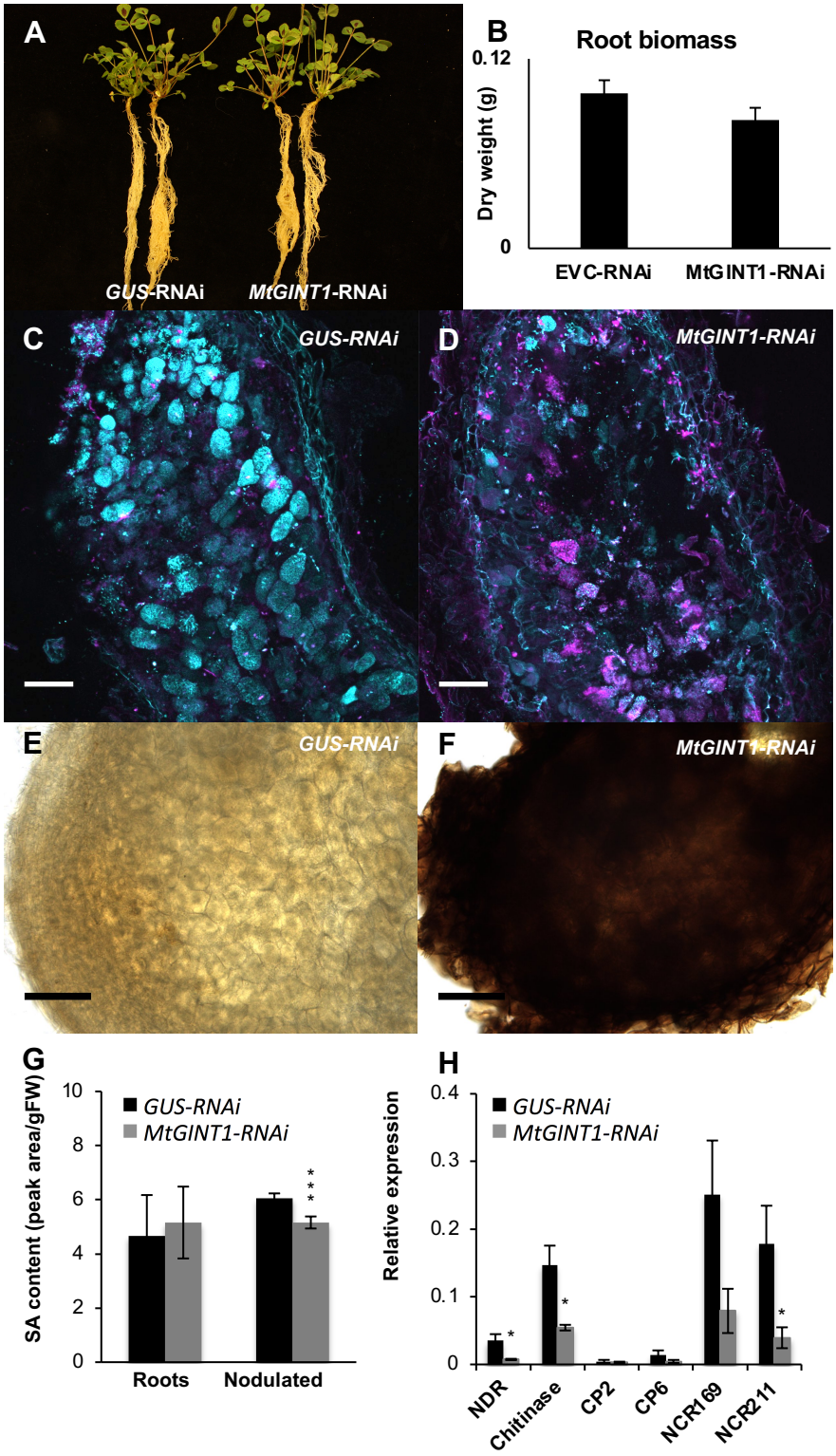

Figure S3. MtGINT1-silencing does not affect root growth or defense response, related to Figure S3. (A) Images of chimeric *RNAi* hairy root plants grown for 4 weeks and fertilized with half-strength MS. **(B)** Quantification of root biomass (dry weight). Error bars reflect ± SEM (*n*=8). **(C and D)** Live/dead staining using Syto 9 (live; cyan) and Propidium iodide (dead; magenta) (scale = 50 µm) in nodules 21 dpi. **(E and F)** H_2O_2 detection in nodules by DAB staining (scale = 100 µm) 21 dpi. **(G)** SA content in uninoculated and nodulated RNAi root systems measured by LC-MS/MS (*n*=3). **(H)** Expression of defense and senescence-associated genes measured by qRT-PCR relative to *MtEF-1a* (*n*=5). Asterisks indicate statistical significance between *MtGINT1-RNAi* and control nodules determined by Student's t-test, (p-value: *< 0.05, **<0.01, ***<0.005). Error bars reflect ± SEM.

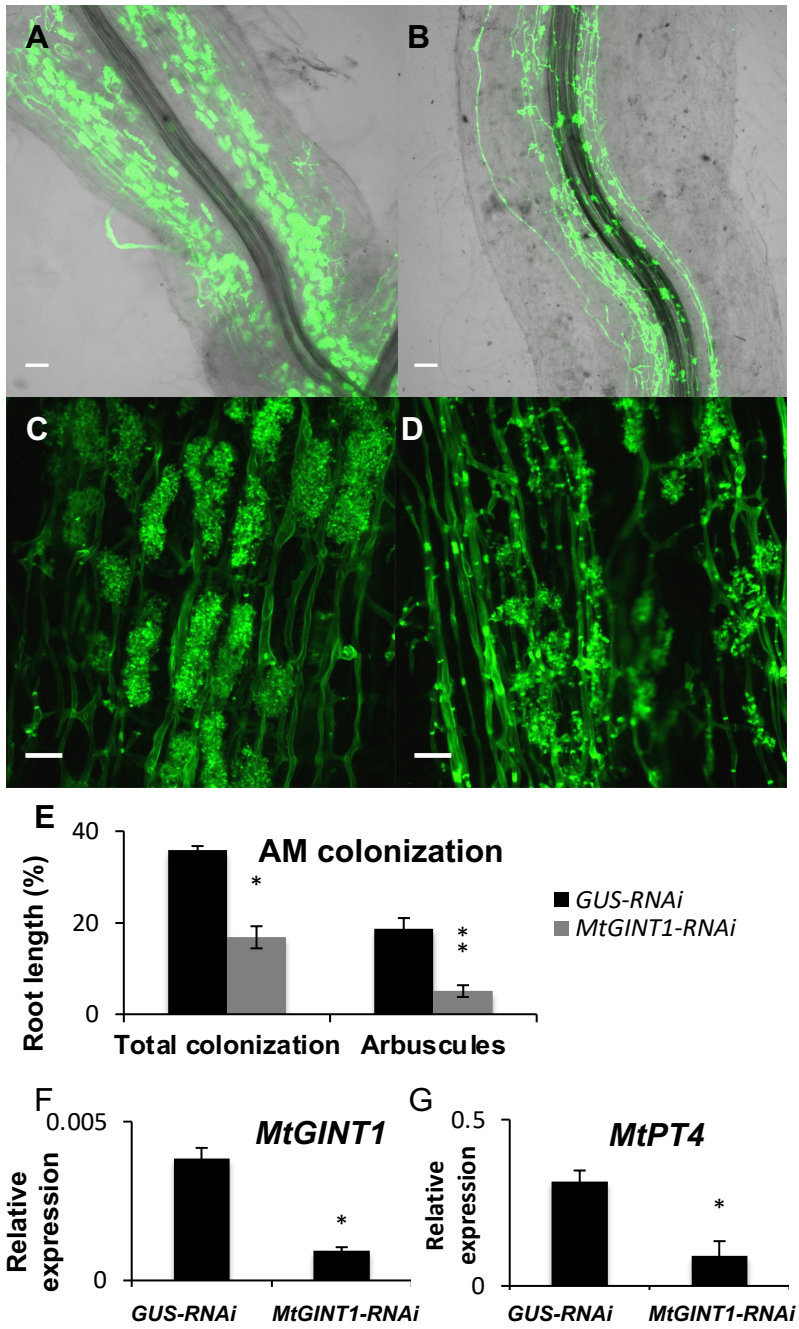

Figure S4. AM colonization is impaired in *p35S:MtGINT1-RNAi* roots at 35 dpi with *R. irregularis*, related to Figure 4. (A-D) Mycorrhized *GUS-RNAi* **(A and C)** and *MtGINT1-RNAi* **(B and D)** roots stained with WGA-488 for fungal chitin (A and B, scale bar = 50 µm; C and D scale bar = 20 µm). **(E)** Quantification of mycorrhizal colonization by on gridline intersect (n=5) represented as the average ± SEM. **(F and G)** *MtGINT1* and *MtPT4* expression measured relative to *MtEF-1α* by qRT-PCR (n=4) ± SEM. Significant differences between *MtGINT1-RNAi* and control roots are indicated by Student's t-test (p-value: *< 0.05, **<0.005).

Primer name	Sequence
MtGINT1-RNAi-F	CCATCTAGAATGGGTTCCGGTCAGATTAG
MtGINT1-RNAi-R	GCATGAATTCCACAAGTCACCACAGGATTC
GUS-RNAi-F	CCATCTAGACTTACGTGGCAAAGGATTCGA
GUS-RNAi-R	GCATGAATTCGAACATTACATTGACGCAGGTG
MtGINT1-RNAiGG-F	ACCAGGTCTCAGGAGATGGGTTCCGGTCAGATTAGC
MtGINT1-RNAiGG-R	ACCAGGTCTCATCGTCACAAGTCACCACAGGATTCG
GUS-RNAiGG-F	ACCAGGTCTCAGGAGCTTACGTGGCAAAGGATTCGA
GUS-RNAiGG-R	ACCAGGTCTCATCGTGAACATTACATTGACGCAGGTG
BsrGI-GINT1-F	TAATGTACAATGGGTTCCGGTCAGATTAGC
BspEI-GINT1-R	TATATCCGGACACAAGTCACCACAGGATTCG
BamHI-GINT1-F	TAAGGATCCATGGGTTCCGGTCAGATTAGC
MluI-GINT1-R	TATAACGCGTCACAAGTCACCACAGGATTCG
MtGINT1-CDS-F	ATGGGTTCCGGTCAGATTAG
MtGINT1-CDS-R	CTATACATCCCAACCATCTCT
MtGINT1-CDSns-R	TACATCCCAACCATCTCTCC
MtGINT1pro-F	AAAAAGCAGGCTCCGTTTCTATCTGACGACAATTCAAGGG
MtGINT1pro-R	GAAGCCATGATTTTTGAAAGGTGGTTTGTGCAG
mCherryBCP1-F	CTTTCAAAAATCATGGCTTCTTCTCGGTAGT
mCherryBCP1-R	GTACAAGAAAGCTGGGTCACTGGATTTTGGTTTTAGGAA
qMtEF1α-F	TGACAGGCGATCTGGTAAGG
qMtEF1α-R	TCAGCGAAGGTCTCAACCAC
qMtPT4-F	GGATTCTTTTGCACGTTCTTGG
qMtPT4-R	CCTGTCATTTGGTGTTGCAGTG
qMtGINT1-F	GTATTTGAGCACAATGGCCAG
qMtGINT1-R	GATAAAGGAATCAATAAGGGGC
qMtGMT1-F	CTAATCAAACCCCTCAAATTCC
qMtGMT1-R	ATCATATCTCTTCCACGTGTTC
qRiTEF-F	TGTTGCTTCGTCCCAATATC
qRiTEF-R	GGTTTATCGGTAGGTCGAG
qMtNDR-F	GGGAAATTGAAGCTTCCCAAAAT
qMtNDR-R	CCTAAACCTAAATTTACAACTACTGCTCC
qMtChitinase-F	GGGCTTGAATGCGGAAGAGG
qMtChitinase-R	CAAGATTGTCTCCATATCCAACTCC
qMtCP2-F	AGTGGATGCCGCTGAAGG
qMtCP2-R	TCAATCACAGTTTTGCTCAAATTAC
qMtCP6-F	GCAATGATGGCATCTTATCCC
qMtCP6-R	TACACAAGCATAATCACAATTTAC
qMtNCR169-F	GGAAATGCGTTGAAAATGTTTGTG
qMtNCR169-F	AACATTTCTCCACTTTATTCTCGGG
qMtNCR211-F	GCGTTAATGCACATCATTTGTGG
qMtNCR211-R	TTATTCTCGGACACAAACACCTTG
qMtMYB1-F	TAAGAGAGTTGATGATGATGTTC
qMtMYB1-R	GATGAGTGATTCTGTTGAACC

Table S1. Primers used in this study. Related to STAR Methods.